Planetary and Space Science 172 (2019) 22–42

Contents lists available at ScienceDirect

Planetary and Space Science

journal homepage: www.elsevier.com/locate/pss

Modelling DESTINY$^+$ interplanetary and interstellar dust measurements en route to the active asteroid (3200) Phaethon

Harald Krüger [a,*], Peter Strub [a,b], Ralf Srama [b], Masanori Kobayashi [c], Tomoko Arai [c], Hiroshi Kimura [c], Takayuki Hirai [c], Georg Moragas-Klostermeyer [b], Nicolas Altobelli [d], Veerle J. Sterken [e], Jessica Agarwal [a], Maximilian Sommer [b], Eberhard Grün [f]

[a] MPI für Sonnensystemforschung, Göttingen, Germany
[b] Institut für Raumfahrtsysteme, Universität Stuttgart, Germany
[c] Planetary Exploration Research Center, Chiba Institute of Technology, Narashino, Japan
[d] European Space Agency, ESAC, Madrid, Spain
[e] Institute of Applied Physics, University of Bern, Switzerland
[f] MPI für Kernphysik, Heidelberg, Germany

A B S T R A C T

The JAXA/ISAS spacecraft DESTINY$^+$ will be launched to the active asteroid (3200) Phaethon in 2022. Among the proposed core payload is the DESTINY$^+$ Dust Analyzer (DDA) which is an upgrade of the Cosmic Dust Analyzer flown on the Cassini spacecraft to Saturn (Srama et al., 2011). We use two up-to-date computer models, the ESA Interplanetary Meteoroid Engineering Model (IMEM, Dikarev et al., 2005a, c), and the interstellar dust module of the Interplanetary Meteoroid environment for EXploration model (IMEX;Sterken et al. 2013; Strub et al., 2019) to study the detection conditions and fluences of interplanetary and interstellar dust with DDA. Our results show that a statistically significant number of interplanetary and interstellar dust particles will be detectable with DDA during the 4-years interplanetary cruise of DESTINY$^+$. The particle impact direction and speed can be used to descriminate between interstellar and interplanetary particles and likely also to distinguish between cometary and asteroidal particles.

1. Introduction

The DESTINY$^+$ (Demonstration and Experiment of Space Technology for INterplanetary voYage Phaethon fLyby and dUst Science) mission has been selected by the Japanese space agency JAXA/ISAS (Kawakatsu and Itawa, 2013; Arai et al., 2018). The mission target is the active near-Earth asteroid (3200) Phaethon (Jewitt and Li, 2010; Jewitt et al., 2013). DESTINY$^+$ will be launched in 2022 initially into a low elliptical Earth orbit. Driven by its ion engine, the spacecraft will raise its altitude until reaching the Moon for a series of gravity assists (Sarli et al., 2018) and will ultimately be injected into a heliocentric trajectory. A flyby at Phaethon is presently planned for August 2026 at a heliocentric distance of 0.87 AU. A later gravity assist at Earth may redirect the spacecraft to another target. The DESTINY$^+$ mission schedule is given in Table 1. DESTINY$^+$ is a three-axis stabilised spacecraft.

The proposed science instruments on board DESTINY$^+$ are two cameras (the Telescopic CAmera for Phaethon, TCAP, and the Multiband CAmera for Phaethon, MCAP; Ishibashi et al., 2018), and the DESTINY$^+$ Dust Analyzer (DDA; Kobayashi et al., 2018). DDA is an upgrade of the Cassini Cosmic Dust Analyzer (CDA) which very successfully investigated dust throughout the Saturnian system (Srama, 2009; Srama et al., 2004, 2011). DDA will be an impact ionization time-of-flight mass spectrometer capable of analyzing sub-micron and micron sized dust particles with a mass resolution of $m/\Delta m \approx 100-150$, and a trajectory sensor. In addition to the elemental and isotopic composition of impacting dust particles the instrument will measure the particle's mass, velocity vector, electrical charge and impact direction. DDA will measure the particle impact speed with an accuracy of approximately 10% and the impact direction with an accuracy of about 10°. This will allow us to constrain the trajectory, and thus, the source body of each detected particle individually (Hillier et al., 2007). As such, the in-situ particle analysis will provide compositional information on the source object where the particles originated. DDA will be equipped with two sensor heads, allowing for the measurement of positively and negatively charged ions released from impacting dust particles.

Phaethon is an extraordinary near-Earth asteroid with a diameter of 5.8 km (Taylor et al., 2018). Its perihelion distance is presently 0.14 AU with an orbital period of 1.433 yr. Around perihelion its surface

* Corresponding author.
E-mail address: krueger@mps.mpg.de (H. Krüger).

https://doi.org/10.1016/j.pss.2019.04.005
Received 19 October 2018; Received in revised form 3 April 2019; Accepted 15 April 2019
Available online 4 May 2019

Table 1
DESTINY$^+$ mission schedule based on the trajectory EAEXX01[a] provided by JAXA/ISAS.

Launch	07 October 2022
Escape from Earth orbit	24 September 2024
(3200) Phaethon flyby	01 August 2026
Earth swing-by	07 October 2028

[a] We use an updated trajectory as compared to the one studied by Sarli et al. (2018).

temperature reaches more than 1000 K. Phaethon is the source of the Geminids, one of the most active meteor showers visible in the Earth's night sky. While parent bodies of meteor showers are mostly comets, Phaethon is an Apollo-type asteroid with a carbonaceous B-type reflectance spectrum, similar to aqueously altered CI/CM meteorites, and of hydrated minerals (Licandro et al., 2007). Recurrent dust ejection and a dust tail were reported at perihelion (Li and Jewitt, 2013; Jewitt et al., 2013), while no coma was observed around 1.0 – 1.5 AU (Hsieh and Jewitt, 2005; Jewitt et al., 2013; Ye et al., 2018; Kimura et al., 2019). Phaethon's dust ejection mechanism remains unknown. Its physical properties were recently summarized by Hanuš et al. (2016). Ground-based observations during a close encounter with Earth in December 2017 showed that Phaethon has a non-hydrated surface (Takir et al., 2018), and the light reflected from its surface shows an unusually strong polarization which may be due to relatively large ($\sim 300\ \mu$m) particles and/or high porosity of the surface material (Ito et al., 2018). Finally, Phaethon shows indications for compositional variations across its surface (Kareta et al., 2018).

DESTINY$^+$ will fly by Phaethon at a distance of 500 km or less, and the DDA instrument will directly analyse dust released from Phaethon's surface (Kimura et al., 2019; Szalay et al., 2019). DDA will investigate the dust trail, the spatial distribution and composition of meteoroids in Phaethon's vicinity, as well as its surface composition and geology.

In addition to the dust measurements at the Phaethon flyby, DDA will be able to measure dust in interplanetary space during its four years of interplanetary voyage between the orbits of Venus and Earth (Fig. 1). Interstellar particles with a radius $r_d \gtrsim 0.1\ \mu$m pass the heliospheric bow shock and enter the heliosphere (Linde and Gombosi, 2000; Slavin et al., 2012; Sterken et al., 2015; Mann, 2010, and references therein). As a consequence, interstellar dust constitutes the dominant known particulate component in the outer solar system (in number flux, not in mass flux).

Interstellar dust particles condense in the extended atmospheres of evolved stars and in stellar explosions and are injected into the interstellar medium. The particles originally carry the elemental and isotopic signatures from the environment where they were formed. Ultraviolet irradiation, interstellar shock waves, and mutual collisions subsequently modify the signatures and deplete particles in the interstellar medium. In dense molecular clouds particles can grow by agglomeration and accretion (see, e.g. Tielens, 2005). In our local environment, the Sun and the heliosphere are surrounded by the diffuse Local Interstellar Cloud (LIC) of warm gas and dust where dust contributes about 1% of the cloud mass. The Sun's motion with respect to this cloud causes an inflow of interstellar matter into the heliosphere (Frisch et al., 1999).

Interstellar dust in the solar system was undoubtedly detected by the Ulysses spacecraft far from the ecliptic plane and outside the inner solar system (Grün et al., 1993). Although the interstellar dust flow is modulated by the Lorentz force, solar radiation pressure and solar gravity (Landgraf, 2000; Sterken et al., 2012, 2013), interstellar dust of some sizes can reach the region inside Earth's orbit (Altobelli et al., 2003, 2005; 2006; Strub et al., 2019; Krüger et al., 2019). A small number of interstellar particles was successfully collected and returned to Earth by the Stardust spacecraft (Westphal et al., 2014), and a few dozen particles were analysed with CDA when Cassini was in orbit about Saturn (Altobelli et al., 2016). See Mann (2010) and Sterken et al. (2019) for comprehensive reviews of interstellar dust in the solar system, the latter

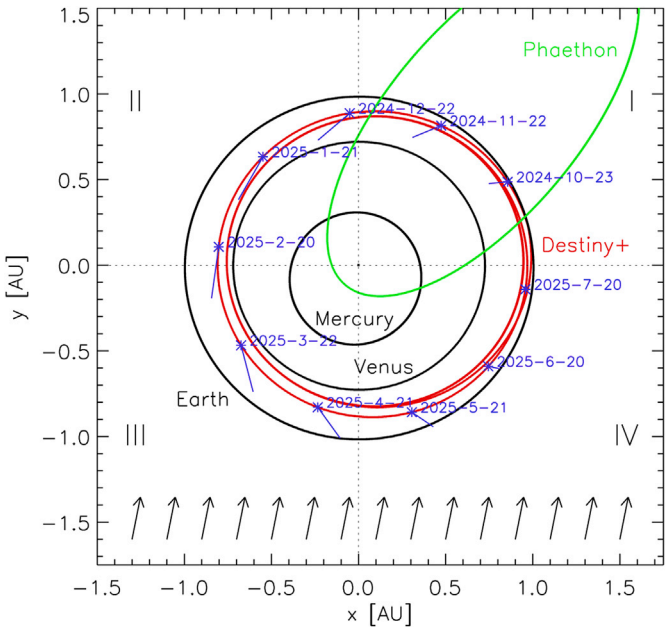

Fig. 1. Trajectories of DESTINY$^+$ (red) and (3200) Phaethon (green) projected onto the ecliptic plane. Black arrows at the bottom indicate the flow of interstellar dust particles with a ratio of solar radiation pressure over gravity $\beta = 1$, which is assumed to be co-aligned with the flow of interstellar neutral helium (Witte et al., 2004,Wood et al., 2015). The approach direction of these particles in the spacecraft-fixed coordinate system is indicated by blue lines for selected times during the first year of the mission, the line length is proportional to the particle impact speed (see also Fig. 3). Vernal equinox is to the right. DESTINY$^+$ trajectory from JAXA/ISAS (EAEXX01), updated from the earlier one studied by Sarli et al. (2016).

with a focus on the last approximately 10 years of research.

These observations open the possibility for spacecraft in the inner solar system like DESTINY$^+$ to detect and analyse interstellar dust in-situ near Earth's orbit (Grün et al., 2005; Strub et al., 2019). The measurements with DDA will address several major open questions in the study of interstellar dust, including: A) Search for complex organic compounds in big – approximately sub-micron and micron-sized – particles (Kimura, 2015); B) Study the variability of particle compositions, also in the context of elemental depletions observed in the interstellar medium (Slavin and Frisch, 2008; Frisch et al., 2011); and C) Investigate the particle dynamics and trajectory modulation in the heliosphere (Sterken et al., 2015).

In addition to the analysis of interstellar dust, the examination of interplanetary dust forming the zodiacal cloud will be another major objective of the DDA measurements. The dominant sources for interplanetary dust in the inner solar system are comets and asteroids (Nesvorný et al., 2010), however, the contributions of each of these sources to the zodiacal dust cloud are still not well known. DDA will be able to measure the dynamical properties of each individual detected particle (Hillier et al., 2007) from an accurate measurement of the particle trajectories. Based on the investigation of the physical properties and the composition of a large number of interplanetary particles DDA will determine the abundances of asteroidal and cometary particles in the zodiacal cloud. This will lead to a better characterisation of the dust sources feeding the zodiacal dust complex and it will ultimately help to improve existing interplanetary dust models (Dikarev et al., 2005a). DDA will also search for dust particles from other sources like the Kuiper belt (Landgraf et al., 2002) or the Oort cloud and may provide information on particle alteration during their voyage to the Earth. A recent review on interplanetary dust was published by Koschny et al., 2019.

In this paper we study the detection conditions for interplanetary and interstellar dust particles with the DDA instrument on board DESTINY$^+$.

Dust detections during the Phaethon flyby are discussed by Kimura et al. (2019) and Szalay et al. (2019). In Section 2 we present simulation results for interplanetary and interstellar dust during the four years of interplanetary voyage of DESTINY$^+$. In Section 3 we discuss the detection conditions for these dust populations, and in Section 4 we summarize our conclusions.

2. Interplanetary and interstellar dust simulations

In this Section we study the detection conditions for interplanetary and interstellar dust particles with the DDA instrument during four years of interplanetary voyage of DESTINY$^+$. To this end, we use two dynamical models developed during the recent years. For modelling interplanetary dust, we use the Interplanetary Meteoroid Engineering Model (IMEM; Dikarev et al., 2005a, c). We simulate interstellar dust with the interstellar dust module of the Interplanetary Meteoroid environment for EXploration model (IMEX; Sterken et al., 2012, 2013; Strub et al., 2019). Both computer models simulate dust densities in interplanetary space, and they are the most up to date models presently available for the dynamics of micrometer and sub-micrometer sized dust in the inner solar system.

In order to calculate dust densities and fluxes along the heliocentric orbit of DESTINY$^+$ we use trajectory data provided by JAXA/ISAS (EAEXX01, cf. Fig. 1; Sarli et al., 2016). The trajectory covers a time period of 1474 days, from 24 September 2024 to 07 October 2028, beginning with the spacecraft's escape from Earth orbit (Table 1). We study fluxes, impact speeds and impact directions on to the DDA sensor, i.e. in the spacecraft-centered reference frame.

We calculate dust fluences from our simulations by assuming a total DDA sensitive area for two sensor heads of 0.035 m^2, and a detection threshold of 10^{-19} kg. For an assumed spherical particle with density typical of astrophysical silicates ($\rho = 3300\,\mathrm{kg\,m^{-3}}$) the detection threshold corresponds to a radius $r_d = 0.02\,\mu$m. Particle fluxes and fluences are given in the spacecraft frame of reference throughout the paper.

2.1. Interplanetary dust

The Interplanetary Meteoroid Engineering Model (IMEM), developed by Dikarev et al. (2005a, c), is the most sophisticated model to predict the dynamics and fluxes of interplanetary dust particles for space missions presently available. It was developed under ESA contract for use by space engineers to study potential dust hazards to interplanetary spacecraft. IMEM simulates the dynamics of five populations of cometary and asteroidal dust as well as interstellar dust in various mass ranges (we use the labelling employed by Dikarev et al., 2005a): (1) Asteroid Collisions ($m \geq 10^{-8}$ kg); (2) Asteroid Poynting-Robertson ($m < 10^{-8}$ kg); (3) Comet Collisions ($m \geq 10^{-8}$ kg); (4) Comet Poynting-Robertson ($m < 10^{-8}$ kg); (5) Interstellar Dust (10^{-18} kg $< m \leq 10^{-12}$ kg).

IMEM was calibrated with infrared observations of the zodiacal cloud by the Cosmic Background Explorer (COBE) DIRBE instrument, in-situ flux measurements by the dust detectors on board the Galileo and Ulysses spacecraft, and the crater size distributions on lunar rock samples retrieved by the Apollo missions. Within the model, the orbital distributions are expanded into a sum of contributions from a number of known sources, including the asteroid belt, with the emphasis on the prominent families Themis, Koronis, Eos and Veritas, as well as comets on Jupiter-encountering orbits (Dikarev et al., 2004, 2005a,c). In order to calculate the particle dynamics, solar gravity and the velocity-dependent tangential component of radiation pressure (Poynting-Robertson effect) are taken into account, while the radial component of solar radiation pressure and the electromagnetic interaction of electrically charged dust particles are neglected.

We do not consider populations 1 (asteroid collisions) and 3 (comet collisions) here because the fluxes of these relatively big particles are very low and, therefore, not relevant in our context. Here we concentrate on particles with masses $m \lesssim 10^{-11}$ kg which corresponds to a particle radius of approximately $r_d \lesssim 10\,\mu$m. The dust mass distributions used by IMEM are shown in Fig. 2. IMEM is a time-independent model, i.e. temporal variations are only introduced by the spacecraft motion around the Sun.

For interstellar dust (population 5) IMEM uses a very simple assumption, i.e. a mono-directional stream of particles with an assumed ratio of gravitational force to solar radiation pressure $\beta = 1$. Because of this simplification we do not use the IMEM interstellar dust module. Instead we use a more realistic model that includes temporal variations in the dust dynamics due to the time-varying interplanetary magnetic field and realistic β values for astronomical silicates (Interplanetary Meteoroid environment for EXploration, IMEX; cf. Section 2.2, see also Strub et al., 2019).

When the Ulysses/Galileo in-situ data were incorporated in the IMEM model simultaneously with the COBE/DIRBE infrared sky maps, these two datasets turned out to be incompatible (Dikarev et al., 2005b). Therefore, the ion charge calibration of the in-situ detectors was revised by a factor of 16, that is to require an impactor 16 times more massive than derived from the standard instrument calibration derived by Grün et al. (1995). This leads to an increase in particle sizes by a factor of 2.5.

2.1.1. Dust flux and impact speed

Up to now there is no detailed information on the spacecraft orientation available for the DESTINY$^+$ mission. For the IMEM simulations we therefore assume that the normal vector of the DDA sensor surface is oriented parallel to the direction of the spacecraft velocity vector all the time (continuous apex pointing). Other sensor orientations may provide higher dust fluxes. As a first step, we assume the sensor to be a flat plate. IMEM allows the inclusion of a detailed model for the sensor field-of-view (FOV).

In Fig. 3 (top panel) we show the average impact speed for interplanetary dust derived from IMEM. The speed modulation is due to the spacecraft motion around the Sun and the limited FOV of the dust sensor. For the asteroidal particles the average speed varies between 4 and 12 km s^{-1}, while that of the cometary particles ranges from 15 to 17 km s^{-1} (see also the sky maps in Figs. 11–15, right columns). The impact speed of cometary particles is larger on average than that of the asteroidal particles due to their higher orbital eccentricities. It implies that, in particular during periods when the impact speed of asteroidal particles is low, the speed measured by DDA can serve as a discriminator between these dust populations.

Simulated dust fluxes of the interplanetary particles are displayed in

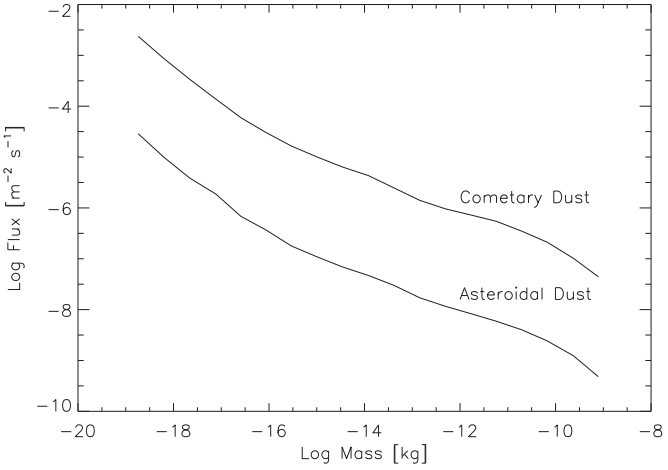

Fig. 2. Mass distributions in the IMEM model (Dikarev et al., 2005a, c) for asteroidal dust (population 2) and for cometary dust (population 4) in the heliocentric distance range traversed by DESTINY$^+$, i.e. between 0.75 AU and 1.0 AU.

the bottom panel of Fig. 3. Their variability is similar to that of the impact speed, this is again due to the spacecraft motion. The flux of asteroidal particles varies by two orders of magnitude while that of the cometary particles varies only by about a factor of 5.

In Fig. 4 we show the same parameters – impact speed and dust flux – but for the DDA sensor FOV (Fig. 5). Again we assumed a sensor pointing parallel to the spacecraft velocity vector. Due to the much narrower FOV of DDA as compared to the flat plate sensor, the dust fluxes are reduced by more than three orders of magnitude. Furthermore, the difference in the average impact speeds between asteroidal and cometary particles is much larger: for asteroidal particles the average speed is below 10 km s^{-1} while that of the cometary particles varies between approximately 30 and 55 km s^{-1}. This supports the discrimination of asteroidal and cometary particles from the impact speed measurement.

Variations in the impact speeds and fluxes are anti-correlated in Figs. 3 and 4, i.e. during periods when high impact speeds occur, the dust fluxes are low, and vice versa, which at first glance seems to be counter-intuitive. Figs. 11–14 in Appendix 1, however, show that particles with different impact speeds approach the spacecraft from different directions which is a consequence of the distributions of orbital elements for the asteroidal and cometary dust particles used in the IMEM model (Dikarev et al., 2004): In the spacecraft frame of reference slow particles are much more abundant than fast particles and one has to keep in mind that particles orbiting the Sun with higher eccentricity and inclination have

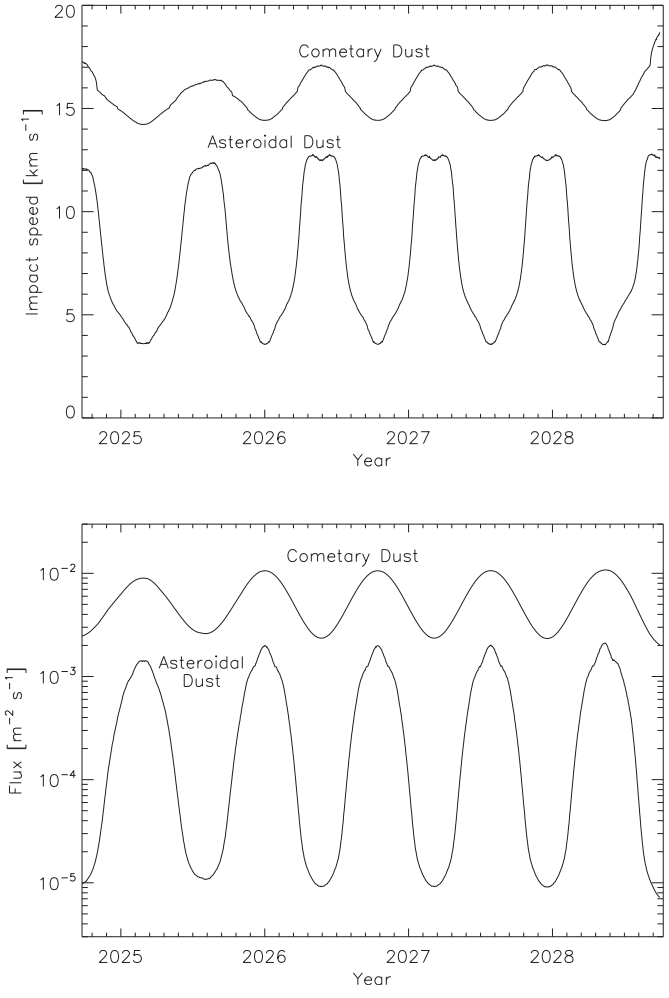

Fig. 3. Average particle impact speed (*top panel*) and flux (*bottom panel*) of asteroidal dust (population 2) and cometary dust (population 4) on to DESTINY^{+} in the spacecraft reference frame, for a flat plate sensor whose normal vector points parallel to the spacecraft velocity vector (continuous apex pointing).

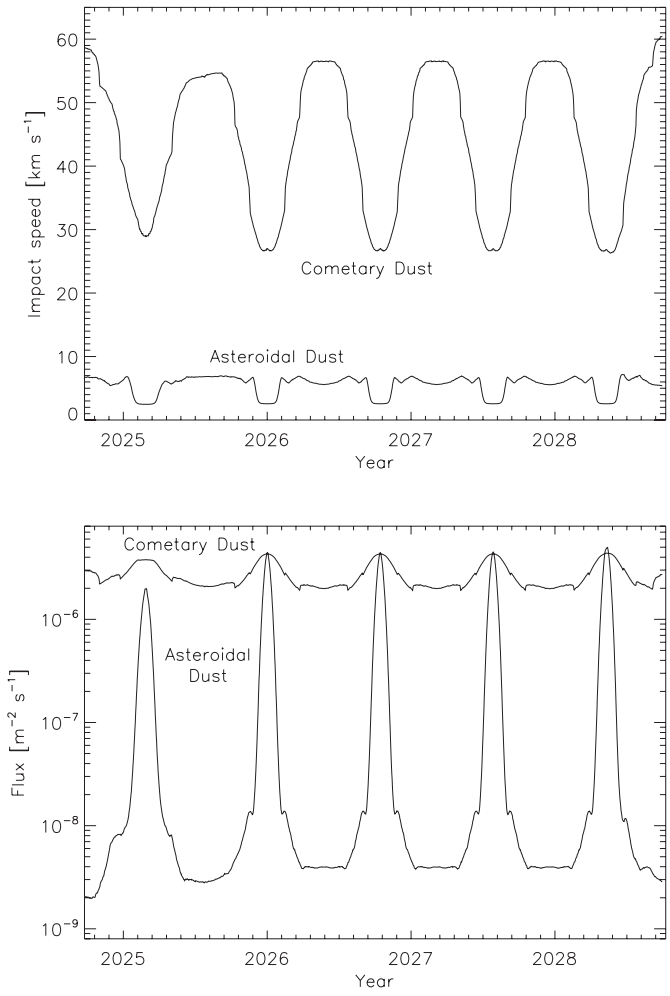

Fig. 4. Same as Fig. 3 but with the DDA sensor characteristics shown in Fig. 5.

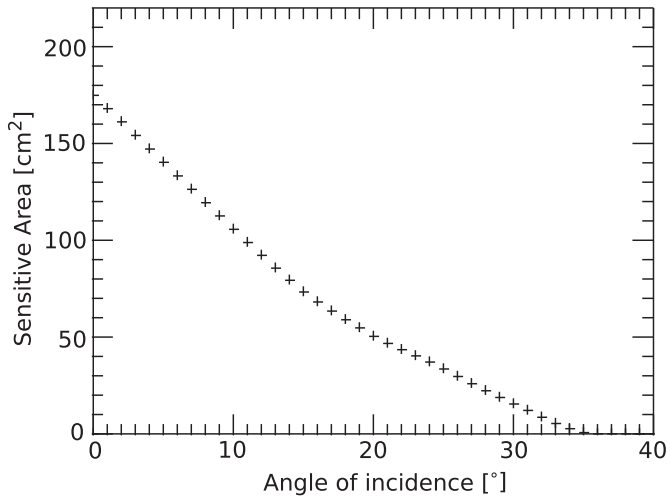

Fig. 5. Field-of-view for DDA used for IMEM and IMEX simulations. The sensitive area refers to a single DDA sensor head.

higher impact speeds. Furthermore, due to the spacecraft motion around the Sun (Fig. 1) the particle impact pattern significantly changes with time. Given that the flat plate sensor, and much more so the narrow-angle DDA sensor, can detect only particles from a very narrow range in impact directions, the sensor cuts out only a very limited fraction of the total

Table 2
Particle detections predicted with IMEM for a mission duration of 1474 days and a sensor normal vector pointing parallel to the spacecraft velocity vector. Column 2 gives the average impact speed, column 3 the average flux, and columns 4 to 6 give the fluence of particles integrated over the entire mission. Column 4 lists the fluence for a 1 m^2 sensor, while columns 5 and 6 give the fluence for a 0.035 m^2 sensor, i.e two DDA sensor heads. Columns 4 and 5 give the fluence for $\pm 90^\circ$ FOV half-cone, column 6 for the DDA sensor (Fig. 5).

Population	Average speed	Average flux	Fluence		
			Flat plate ($\pm 90^\circ$)		DDA
	[km s^{-1}]	[m^{-2} s^{-1}]	[m^{-2}]	[0.035 m^{-2}]	
(1)	(2)	(3)	(4)	(5)	(6)
Asteroidal dust, pop. 2	7.8	$5.4 \cdot 10^{-4}$	$6.8 \cdot 10^{4}$	2380	75
Cometary dust, pop. 4	15.7	$5.7 \cdot 10^{-3}$	$7.3 \cdot 10^{5}$	25550	685
Total interplanetary dust	11.7	$6.3 \cdot 10^{-3}$	$8.0 \cdot 10^{5}$	27930	760

number of particles approaching the spacecraft, which are concentrated in the center of the plots shown in Figs. 11–14.

We also performed test runs with the IMEM model simulating dust fluxes on to the Earth. Due to the rotational symmetry of the interplanetary dust cloud implemented in the model and the practically circular Earth orbit with zero inclination, these simulations did not show a temporal variation, neither for a spherical (4π) nor a flate plate (2π) sensor, as expected. The temporal modulation only appears in the simulation runs with the DESTINY$^+$ trajectory.

2.1.2. Dust fluences

In this subsection we give estimates for dust fluences detectable with DDA during the DESTINY$^+$ mission derived from our IMEM simulations (Table 2). A flat plate sensor has been assumed for most of our simulations so far, i.e. the sensor has a FOV of $\pm 90^\circ$, and its sensitivity profile as a function of incidence angle is described by a cosine function. Note that DDA will have an angular sensitivity considerably smaller than that of a flat plate (Fig. 5).

Next we study the effect of the FOV on the dust fluences. To this end, we perform IMEM simulations assuming a flat plate sensor whose normal vector is oriented parallel to the spacecraft velocity vector as before. This time, however, we vary the FOV. The result is shown in Fig. 6[1]. It is obvious that the dust fluences are significantly reduced for a narrower FOV.

Finally, we use the DDA sensitivity profile (Fig. 5) to simulate dust fluences, again with a sensor pointing parallel to the spacecraft velocity vector. The result is listed in Table 2, column 6. The simulations predict a total number of approximately 760 interplanetary particles detectable with two DDA sensor heads during the entire DESTINY$^+$ mission, about 90% of them being of cometary origin. Note that the sensor pointing was not optimised to maximise the dust fluences, see Section 3.

2.2. Interstellar dust

Previous simulations of interstellar dust in the solar system described the interstellar dust flow at larger heliocentric distances well, but they did not have the resolution to enable a good time-resolved description of the dust environment at Earth (Grün et al., 1994; Landgraf, 2000; Sterken et al., 2012).

Based on these earlier models and the dust measurements by the Ulysses spacecraft, Strub et al. (2019) executed high-resolution

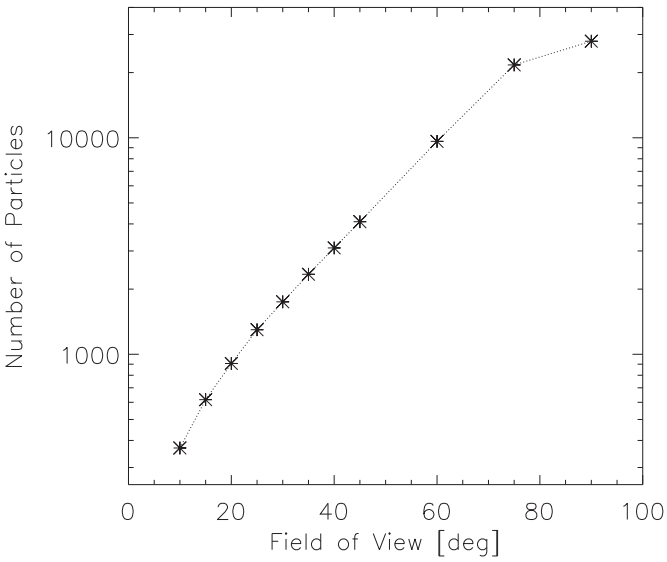

Fig. 6. Fluence of interplanetary dust particles for a flat plate sensor with 0.035 m^2 sensor area and varying sensor FOVs from IMEM simulations. The DDA field-of-view corresponds to an angle of 17° in this diagram.

simulations in the context of the IMEX modelling effort (Interplanetary Meteoroid environment for EXploration) under ESA contract that included an interstellar dust module developed for this purpose. The authors simulated the dynamics of charged micrometer and sub-micrometer sized interstellar particles exposed to solar gravity, solar radiation pressure and a time-varying interplanetary magnetic field (IMF). The size distribution is represented by 12 particle radii between 0.049 μm and 4.9 μm, and the dynamics of each of these sizes was simulated individually, assuming the adapted β-curve for astronomical silicates (Sterken et al., 2012). In IMEX, the dust density in the solar system is calibrated with the Ulysses interstellar dust measurements, again individually for each size bin (Strub et al., 2015). Due to the variable IMF, the IMEX model is time-dependent, contrary to IMEM (Section 2.1). For details of IMEX the reader is referred to Strub et al. (2019). We use IMEX to simulate the time-resolved flux and dynamics of interstellar dust particles in the inner solar system, assuming the DDA sensor profile shown in Fig. 5 with the sensor being oriented towards the effective approach direction of the interstellar particles integrated over all dust size bins.

The IMEX model uses the same initial conditions as Landgraf (2000) and Sterken et al. (2012, 2013): The simulated interstellar particles enter the solar system at a uniform direction and velocity, with an initial velocity of $v_\infty = 26 \mathrm{kms}^{-1}$ and an inflow direction from an ecliptic longitude $\lambda_{ecl} = 259^\circ$ and ecliptic latitude $\beta_{ecl} = 8^\circ$.[2] This is compatible with the inflow direction of the neutral gas into the solar system (Witte et al., 1996; Lallement and Bertaux, 2014; Wood et al., 2015), and it is also compatible with the Ulysses measurements of the interstellar dust flow (Frisch et al., 1999; Strub et al., 2015; Kimura et al., 2003a, b). It is equivalent to the interstellar particles being at rest with respect to the local interstellar cloud surrounding our solar system. In the following we will call this direction the nominal interstellar dust flow direction.

Measurements of interstellar dust inside the planetary system now

[1] In Fig. 6, to describe the sensitive area as a function of incidence angle, we use a cosine function which is cut off at the specific angle given on the x axis of that Figure. This leads to somewhat higher fluences than those derived with the DDA sensitivity profile for a comparable FOV.

[2] Working values of a speed of 25.4km s^{-1} with directions from 255.7° ecliptic longitude and +5.1° ecliptic latitude were recently suggested from Energetic Neutral Atom measurements by the Interstellar Boundary EXplorer mission (IBEX) by McComas et al. (2015) and confirmed by Swaczyna et al. (2018). These values agree with the speed of $24.5^{+1.1}_{-1.2}$ km s^{-1}, the ecliptic longitude of $252 \pm 5^\circ$ and the ecliptic latitude of $5 \pm 5^\circ$ for the initial condition of the interstellar dust stream found by Kimura et al. (2003b).

provide a new window for the study of solid interstellar matter at our doorstep (Frisch et al., 1999). The flow of the interstellar particles in the heliosphere is governed by two fundamental effects: (1) the combined gravitational and radiation pressure force of the Sun, and (2) the Lorentz force acting on a charged particle moving through the solar magnetic field "frozen" into the solar wind (the IMF). The former effect can be described as a multiplication of the gravitational force by a constant factor $(1-\beta)$, where the radiation pressure factor $\beta = |\mathbf{F}_{rad}|/|\mathbf{F}_{grav}|$ is a function of particle composition, size and morphology. Interstellar particles approach the Sun on hyperbolic trajectories, leading to either a radially symmetric focussing ($\beta < 1$) or defocussing ($\beta > 1$) downstream of the Sun which is constant in time (Bertaux and Blamont, 1976; Landgraf, 2000; Sterken et al., 2012). Particle sizes observed by the Ulysses dust detector typically range from approximately 0.1 μm to several micrometers, corresponding to $0 \lesssim \beta \lesssim 1.9$ (Kimura et al., 2003a; Landgraf et al., 1999).[3] A detailed description of the forces acting on the particles and the resulting general interstellar dust flow characteristics was given by Sterken et al. (2012).

The interplanetary magnetic field (IMF) shows systematic variations with time, including the 25-day solar rotation and the 22-year solar magnetic cycle, as well as local deviations due to disturbances in the interplanetary magnetic field, due to, e.g. coronal mass ejections (CMEs). The dust particles in interplanetary space are typically charged to an equilibrium potential of +5 V (Mukai, 1981; Kimura and Mann, 1998; Kempf et al., 2004). Small particles have a higher charge-to-mass ratio, hence their dynamics is more sensitive to the interplanetary magnetic field. The major effect of the magnetic field on the charged interstellar dust is a focussing and defocussing relative to the solar equatorial plane with the 22-year magnetic cycle of the Sun (Landgraf, 2000; Landgraf et al., 2003; Sterken et al., 2012, 2013). Modifications of the particle dynamics by solar radiation pressure and the Lorentz force acting on charged dust particles have to be taken into account for a proper interpolation of the interstellar dust properties to the interstellar medium outside the heliosphere where these particles originate from (Slavin et al., 2012).

In Figs. 7–9 we show the temporal variations of the dynamical parameters for particles in three representative size bins. Along the DESTINY$^+$ trajectory the dust spatial density and dynamical parameters of the interstellar particles depend on spacecraft position, time in the solar (Hale) cycle and particle size. At this distance from the Sun, each size range is dominated by a different force (Landgraf, 1998; Sterken et al., 2012; Strub et al., 2019): Electromagnetic interaction ($r_d = 0.072$ μm), radiation pressure (0.335 μm), and solar gravity (0.492 μm). Dust spatial densities in the inner solar system for these particle sizes during the DESTINY$^+$ mission are shown in Figs. 16–18 in Appendix 2.

Strong modulations of the dust impact rate over time are obvious in Figs. 7–9. To first order, maxima and minima are caused by the approximately annual periodicity of the spacecraft motion around the Sun, and by the varying particle impact speed (see Fig. 1): When the spacecraft moves against the dust flow (approximately in quadrants II and III) the impact speed reaches up to 60 km s^{-1}, while at other times it is close to zero (at $Y \approx 0$ in quadrants I and IV). Fluxes and impact speeds are highly correlated, high fluxes coincide with high impact speeds.

In addition to this modulation by the spacecraft motion, size-dependent forces acting on the particles lead to further alterations as described above. Particles with $r_d \lesssim 0.1$ μm strongly interact with the IMF (Fig. 7, top panel). Therefore, the phase of the 22-year IMF cycle strongly affects their spatial density and flow: In 2022 the overall configuration of the IMF will change from a defocussing to a focussing configuration, and it is expected to reach its maximum focussing condition approximately in 2031. It leads to an overall increase in the spatial density of these small particles in the inner solar system and, hence, to an increase in the impact rate during the DESTINY$^+$ mission, in addition to the approximately annual modulation caused by the spacecraft motion alone. This is evident by the increase in the dust density seen in the left column of Fig. 18 in the Appendix. Even under optimal focussing conditions of the IMF, strong filtering of the heliosphere remains effective for these particles, and the flux at Earth's orbit is reduced by orders of magnitude with respect to the unfiltered flux outside the heliosphere (Landgraf et al., 2000; Krüger et al., 2015).

Interstellar particles with a ratio of solar radiation pressure over gravity $\beta > 1.4$ cannot be observed at Earth orbit because the solar radiation pressure prevents them from entering the inner solar system (the avoidance cone due to radiation pressure filtering is seen in the left and middle columns of Fig. 17 in Appendix 2). We use the same β-curve as Sterken et al. (2013) which was adapted from the curve for astronomical silicates given in Gustafson (1994), by scaling it to a maximum value $\beta_{max} \simeq 1.6$, in agreement with the range $1.4 \lesssim \beta_{max} \lesssim 1.8$ measured by Ulysses (Landgraf et al., 1999). For this assumption, particles with sizes $0.1\ \mu m \lesssim r_d \lesssim 0.3\ \mu m$ have $\beta > 1.4$ and are absent at Earth orbit. In the simulations, this applies to particles in the size bins $r_d = 0.156$ μm and 0.229 μm, and partially to particles with $r_d = 0.106$ μm which are detectable only during short periods of time. On the other hand, particles with $r_d \gtrsim 0.335$ μm can enter the inner solar system and are detectable by DDA.

Finally, the dynamics of particles with $r_d \gtrsim 0.5$ μm are dominated by solar gravity. For these particles the modulation in the impact rate is due to the varying impact speed and gravitational focussing in the downstream region of the interstellar dust stream behind the Sun. Strong enhancements in the impact rate in these regions are shown in Fig. 9. For a more detailed discussion of the particle dynamics at 1 AU heliocentric distance see Strub et al. (2019).

In Figs. 7–9 the third and the forth panels show the deviation of the average particle impact direction from the nominal direction of the interstellar dust flow. Gradual shifts occur in ecliptic longitude for all three particle sizes. These shifts are more or less coincident in time so that, on average, all particles with all three sizes approach from approximately the same direction. Thus, with a sufficiently large FOV, DDA may detect all particle sizes simultaneously.

The bottom panel in Figs. 7–9 shows the 1σ width of the interstellar dust stream. During periods of highest particle impact speeds the interstellar dust stream is narrowly collimated to within less then 10°, while during periods of low speeds the stream width can reach 30°, even and up to 60° for the 0.723 μm particles.

The fluence of interstellar dust particles during the entire DESTINY$^+$ mission is shown in Fig. 10. The gap in the size range $0.1\ \mu m \lesssim r_d \lesssim 0.3\ \mu m$ is due to the radiation pressure filtering in the inner heliosphere, and the drop in the smallest size bin with $r_d = 0.049$ μm is caused by electromagnetic filtering, consistent with the Ulysses dust measurements between 3 and 5 AU (Landgraf et al., 2000; Krüger et al., 2015). During the total measurement period of 1474 days our simulations predict a total number of approximately 170 interstellar particles detectable with two DDA sensor heads having a total sensitive area of 0.035 m^2.. For particles with $r_d \gtrsim 1$ μm the predicted fluence is below one particle impact during the entire DESTINY$^+$ mission, and we therefore do not consider such relatively big particles here.

3. Discussion

A prerequisite for obtaining the dust fluences given in Section 2 is that DDA continuously measures these dust populations. In a real mission scenario, having a dust instrument with a restricted field-of-view, the instrument pointing has to be optimised for each dust population individually, i.e. cometary, asteroidal, and interstellar dust. This implies that lower dust fluences will likely be achieved in reality, unless more than one population can be detected simultaneously with the same instrument pointing. This will be the case with DDA during some mission periods

[3] Landgraf et al. (1999) found a range of $1.4 < \beta < 1.8$ from Ulysses measurements, and Kimura et al. (2003a) found values for β between 0 and 1.9.

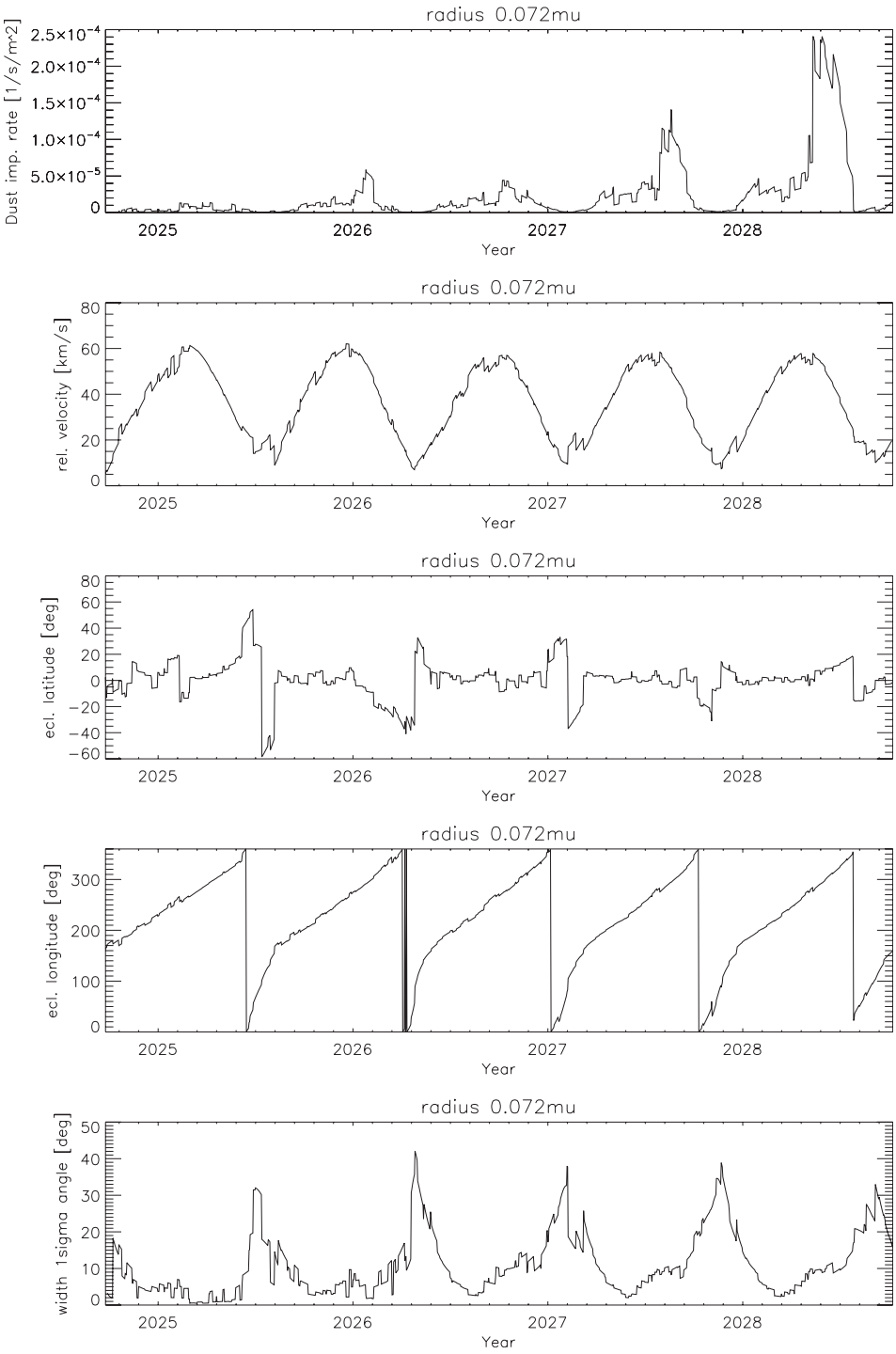

Fig. 7. Simulated impact rate, and dynamical parameters for particles with radius $r_d = 0.072\ \mu$m in the spacecraft reference frame. From top to bottom: impact rate, impact velocity, average approach direction of particles in ecliptic latitude β_{ecl} and ecliptic longitude λ_{ecl}, and the 1 σ width of the interstellar dust flow (note that for calculating impact rates the model uses the DDA sensor profile oriented towards the effective interstellar dust flow direction integrated over all particle size bins).

because the range in impact directions of the interplanetary impactors is much wider than that of interstellar particles. Given the variability of the expected dust fluxes, the measurement periods and instrument pointing scenarios have to be optimised in order to maximise the overall number of measured dust particles for all populations.

Our simulations assumed a sensor pointing parallel to the spacecraft speed vector in the case of interplanetary dust (IMEM) and towards the average interstellar dust inflow direction in the spacecraft reference frame (IMEX), respectively. An optimised pointing scenario, for example performing scans through the dust approach directions expected for different populations in order to derive their relative abundances, will increase the number of interplanetary particle detections. More realistic predictions for dust fluences measurable with DDA require a detailed scenario for the spacecraft orientation during the DESTINY$^+$ mission.

3.1. Interplanetary dust

IMEM was designed as a tool to predict hazards imposed by dust particles on to Earth orbiting and interplanetary spacecraft. Sub-micrometer sized particles which are most susceptible to radiation

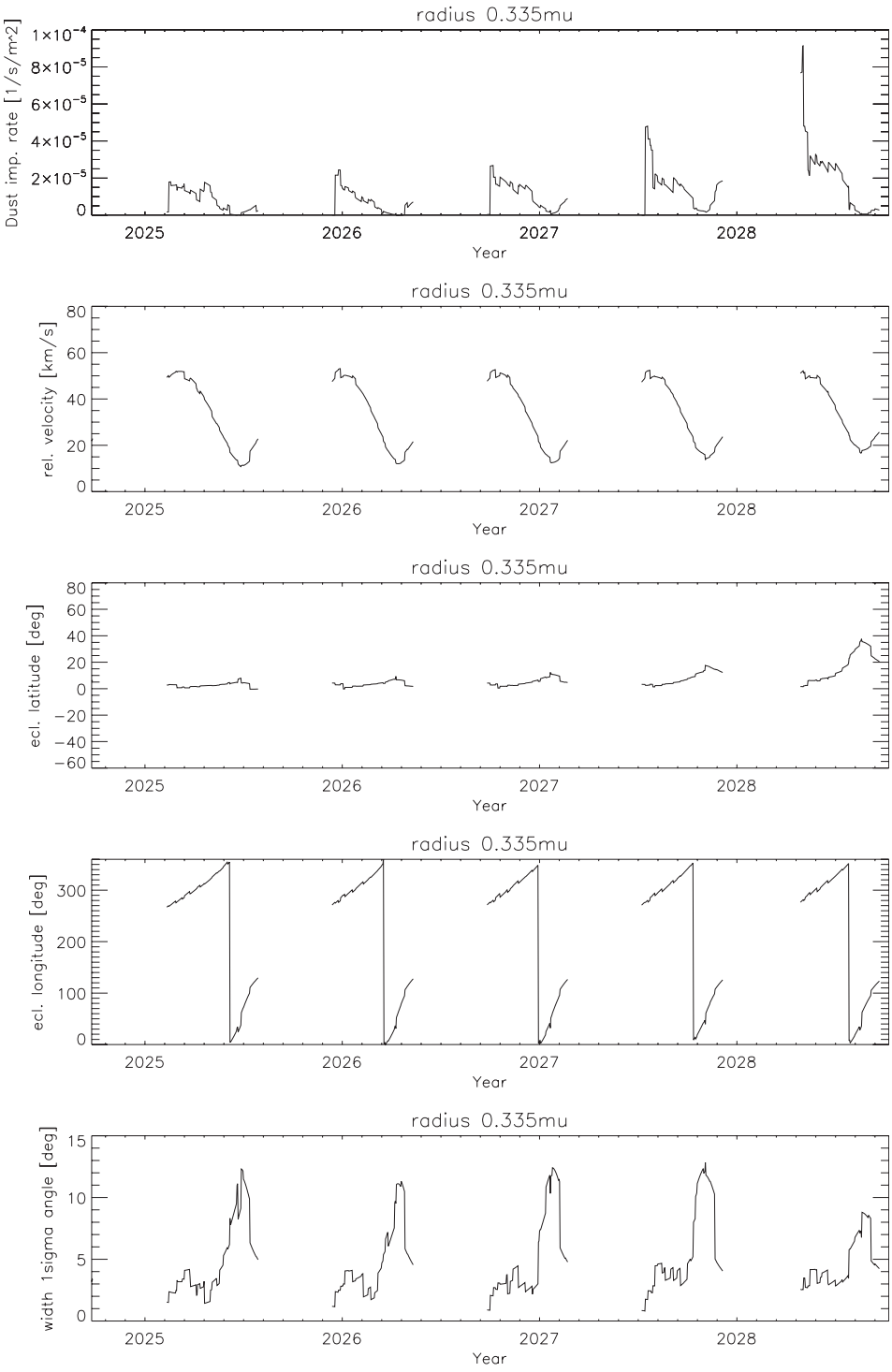

Fig. 8. Same as Fig. 7 but for particle radius $r_d = 0.335\ \mu$m.

pressure usually impose a negligible threat to spacecraft structures. Therefore, the radiation pressure force was not included in IMEM when the model was designed. This leads to uncertainties in the impact directions of dust particles with a high ratio of radiation pressure force over gravity, β. Their range in impact directions is likely much wider than predicted by our simulations so that the measurable fluxes of submicrometer sized particles could be lower than predicted by the IMEM model.

The cometary populations implemented in IMEM are limited to Jupiter Family Comets (JFCs), thus our flux computations are a conservative lower estimate. Dust particles released by Halley-type comets (HTCs) or Oort Cloud type comets (OCCs) can produce particles on heliocentric retrograde orbits. The abundance of retrograde particles around 1 AU can be as high as 10% of the abundance of prograde particles (Nesvorný et al., 2010; Pokorný et al., 2014) for an impact velocity of about 3 times the values derived for the JFCs. Hence, the flux of particles of cometary origin along the trajectory of the spacecraft could be up to 30% higher than computed with IMEM.

Fig. 4 (top panel) shows that a distinction between asteroidal and cometary dust can be accomplished from the particle impact speed: asteroidal dust has average speeds below 10 km s^{-1}, while the average

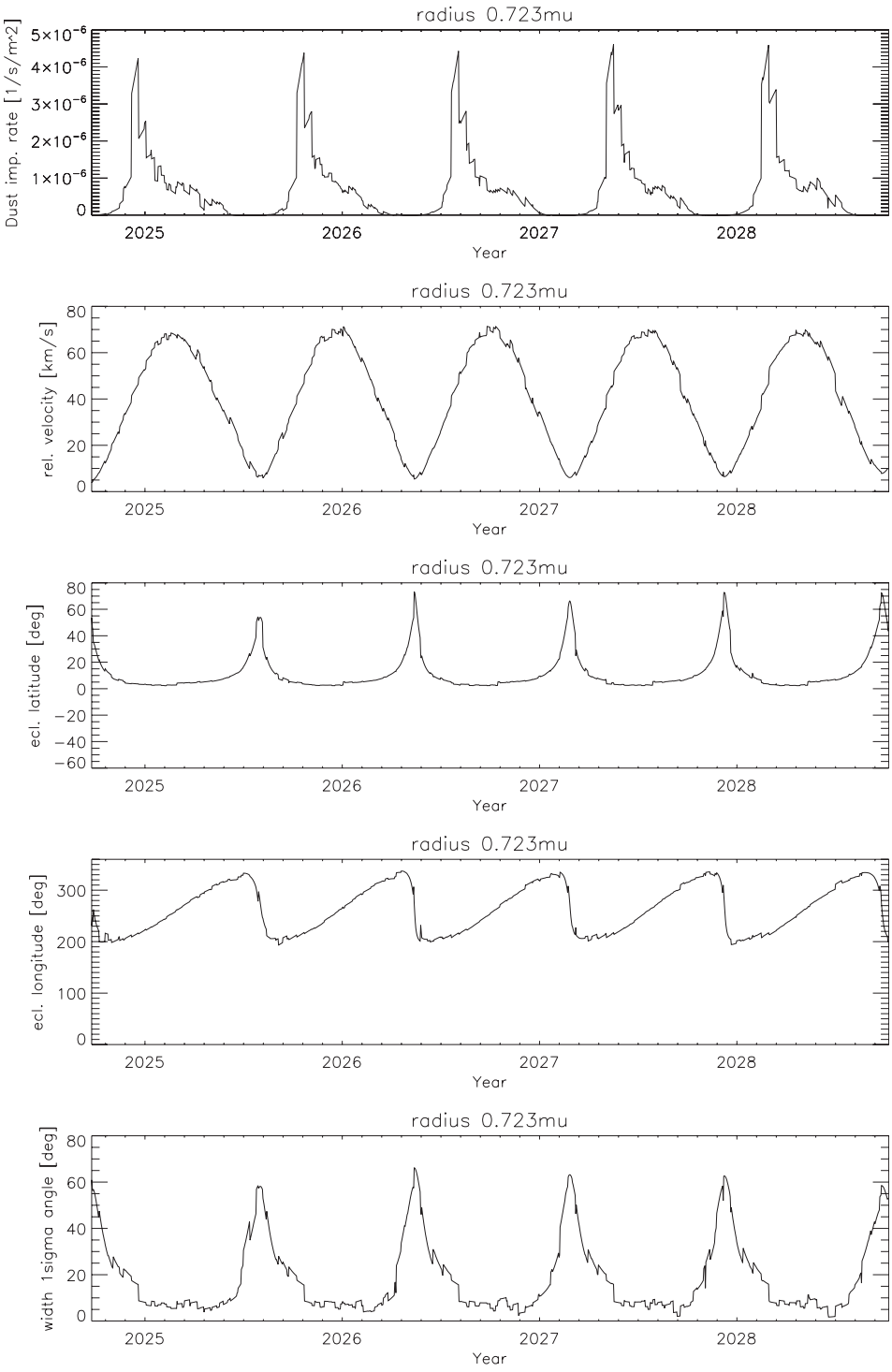

Fig. 9. Same as Fig. 7 but for particle radius $r_d = 0.723\,\mu$m.

speed of cometary particles exceeds 30 km s^{-1}. Inspection of the bottom panel of Fig. 4 reveals that time intervals with the highest fluxes of asteroidal dust approximately coincide with periods of increased interstellar dust flux (Figs. 7–9). Given that the impact speeds of interstellar particles exceed 40 km s^{-1} in these time intervals, a distinction between asteroidal and interstellar particles will be possible from the impact speed and particle sizes during these periods. On the other hand, interstellar and cometary particles have comparable impact speeds and they have to be distinguished preferentially from the particle composition. Considering the number of asteroidal particle detections expected from the IMEM simulations, DDA should be oriented towards the asteroidal particles during these time intervals (spikes in Fig. 4 bottom panel, $Y \approx 0$ in quadrant II in Fig. 1).

On the other hand, cometary particles will be detectable with a relatively constant flux throughout the mission. They should preferentially be measured during time intervals when the expected fluxes of interstellar particles and of asteroidal particles are low (quadrants I and IV in Fig. 1). Based on the expected accuracy of the particle trajectory measurement with DDA, the measurements will allow us to constrain the source body from a backward tracing of the particle trajectory (Hillier et al., 2007). Together with improved modelling of the particle dynamics,

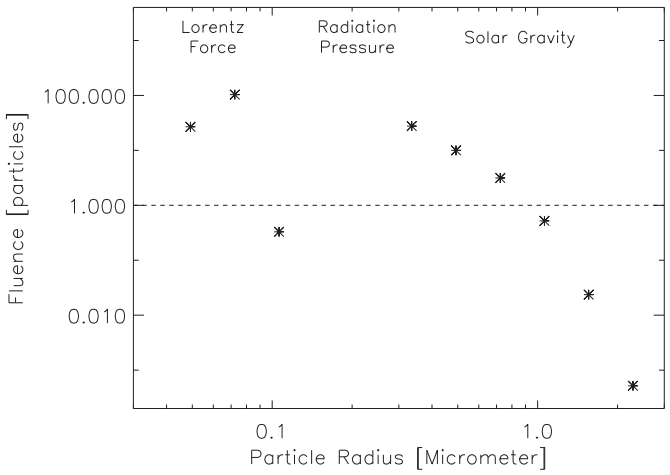

Fig. 10. Fluence of interstellar particles during the 1474 days of the DESTINY$^+$ mission for a sensor area of 0.035 m^2 with DDA pointing in the effective interstellar dust flow direction in the spacecraft based reference frame. The horizontal dashed line indicates the limit of one particle impact detectable during the entire DESTINY$^+$ mission. The approximate size regimes where the different forces dominate the dynamics and, thus, the spatial dust densities are indicated at the top.

we will be able to derive the abundance of asteroidal and cometary particles and, hence, the contributions of each of these dust sources to the zodiacal cloud.

3.2. Interstellar dust

The Ulysses interstellar dust data set was chosen as the calibration dataset for IMEX because it contains the most comprehensive and homogeneous measurements by a single instrument over a period of 16 years, covering a large portion of the 22-year solar cycle. With a total of more than 900 identified interstellar particles it has by far the largest dataset of all interstellar dust measurements performed to date (Krüger et al., 2010, 2015, 2019).

Concerning the normalisation of the simulated fluxes, the temporal variability of the flux and of the flow direction of the interstellar particles in the Ulysses dataset are not entirely reproduced by the model. Therefore, only the overall flux for each particle size bin was taken into account for the normalisation, and each bin was calibrated individually. For most of the Ulysses measurement intervals the model reproduces the dataset within a factor of 2 (Krüger et al., 2019), only in 2005 is the discrepancy more pronounced when a rapid change in interstellar dust flow direction and density was observed (Krüger et al., 2007). The reason for this shortcoming remains an open question at the moment. It may be related to the material properties of the interstellar particles (e.g. composition and porosity), variable particle charging or the particle interaction with the heliospheric boundary (Sterken et al., 2015), or it may be due to changes in the configuration of the heliospheric current sheet which are not taken into account in the present model. This likely marks the limits of our current understanding of the interstellar dust flow through the heliosphere.

Variations in the impact direction and the width of the interstellar stream were measured with Ulysses between 3 AU and 5 AU heliocentric distance (Strub et al., 2015). The authors separated the data set into two subsets, one with particles smaller than about 0.24 μm, and the other one with larger particles. Their analysis showed that most of the time the average impact direction of the larger particles remained within approximately $\pm 20^\circ$ of the undisturbed interstellar dust flow direction, while the directions of the smaller particles frequently deviated by up to 60°, sometimes exceeding 90° (Strub et al., 2015, their Tables 4 and 5). The stream widening for the large particles remained below 10° most of the time, while that of the small particles usually stayed below 30°. It indicates that the interstellar dust stream is rather collimated, consistent with our modelling results for DESTINY$^+$ (Section 2.2).

We also compared the IMEX model predictions to interstellar dust flux measurements from other missions, i.e. Helios, Cassini, and Galileo (Krüger et al., 2019). Despite different heliocentric distance ranges covered by these missions and different detection geometries of the instruments, the model predictions (based on a calibration using Ulysses data) agree with the measured fluxes to within about a factor of 2–3. Typically, the model underestimates the measured dust fluxes. Because of this, and the fact that the interstellar dust stream is rather collimated, the dust fluxes predicted for DESTINY$^+$ by the IMEX model should also be realistic to within a factor of 2, with a tendency to underestimate the true fluxes. The largest uncertainties arise for the small particles because they are most strongly affected by the heliospheric filtering (Landgraf et al., 2000). Our present model assumes an undisturbed heliospheric current sheet which is a good approximation for the IMF during solar minimum conditions, while at solar maximum Coronal Mass Ejections (CMEs) can significantly disturb the IMF, preferentially affecting the dynamics of small particles.

When Cassini was in orbit around Saturn, the CDA instrument also measured interstellar particles for limited periods of time (Altobelli et al., 2016). Only relatively small particles with masses below approximately $5 \cdot 10^{-16}$ kg (corresponding to a particle radius $r_d \approx 0.35\ \mu$m) could be measured because of the limited instrument sensitivity (i.e. instrument saturation for bigger particles). The measured mass spectra show a depletion of carbon, indicating that organic constituents may be rare or even absent in these particles. A carbon depletion in dust in the local interstellar cloud (LIC) was suggested from derived gas-mass abundances (Slavin and Frisch, 2008). Loss of carbon from the dust may occur due to particle destruction by shock waves in the LIC (Kimura, 2015).

The Stardust mission revealed seven interstellar particles which are diverse in elemental composition, crystal structure, and size. The presence of crystalline grains and multiple iron-bearing phases, including sulfide, in some particles indicates that individual interstellar particles diverge from any one representative model of interstellar dust inferred from astronomical observations and theory (Westphal et al., 2014). The Stardust particles also showed that interstellar dust with mass $3 \cdot 10^{-15}$ kg might be porous and has higher β and charge-to-mass ratios (Sterken et al., 2014). Interstellar dust with mass exceeding $5 \cdot 10^{-16}$ kg might be porous aggregates of submicron-sized silicate grains (Sterken et al., 2015; Kimura, 2017). Silicate grains do not stick to each other in the interstellar medium, but organic matter would assist them in sticking, if their surfaces are covered by organic matter. Therefore, submicrometer-sized grains in porous aggregates might still retain organic matter.

Micrometer-sized porous particles generally have higher charge-to-mass ratios (Ma et al., 2013) and higher β values (Kimura and Mann, 1999) than compact particles of the same mass. With DDA we will be able to measure the electrical charge and mass of interstellar particles in much the same way as was successfully done for interplanetary dust particles with Cassini CDA (Kempf et al., 2004). Hence, these parameters together with the measured dust spatial densities and dynamical modelling will better constrain the particle porosities in the future.

Gravitational focussing deflects and concentrates particles whose dynamics are dominated by the gravitational field of a celestial body. In the case of the interstellar dust stream in the solar system, particles with $r_d \gtrsim 0.5\ \mu$m are concentrated in the downstream direction behind the Sun (Fig. 16; $X \gtrapprox 0$ in quadrant I in Fig. 1). The interstellar dust flow is inclined by 8° with respect to the ecliptic plane, so that DESTINY$^+$ will not traverse the region with the highest dust density (see the middle panel of Fig. 16).

Even though an increased dust impact rate is expected in this region (the spikes in Fig. 9, top panel), the detection of only 14 bigger interstellar particles is predicted in the size range $0.5\ \mu\text{m} \lesssim r_d \lesssim 1.0\ \mu$m during

the entire DESTINY$^+$ mission. This number takes into account that the spatial density of such particles is enhanced in the region downstream of the Sun, due to focussing by solar gravity (see Fig. 16 in Appendix 2, and the spikes in the top panel of Fig. 9). Hence, the DDA pointing should be optimised for the detection of such big particles preferentially during the time intervals when DDA will traverse this region (at $X \gtrapprox 0$ in quadrant I in Fig. 1). The gravitational focussing increases the impact speed to about 40 to 50 km s^{-1} in this region (Fig. 9, second panel from top), however, these high speeds are expected to restrict the detectability of organic compounds in the DDA impact spectra because complex organic molecules are mostly destroyed (Khawaja, 2016). Another limitation is imposed by the DDA sensor itself: In order to avoid abundant noise events in the data set, the angle between the instrument boresight and the Sun direction has to exceed 90° according to the present instrument design, restricting the detectability of interstellar dust in this spatial region downstream of the Sun.

A comparison of Figs. 16 and 17 in Appendix 2 shows that the spatial distribution of the intermediate sized particles with $r_d = 0.335\,\mu$m is completely different from that of the larger $r_d = 0.723\,\mu$m particles: While the larger particles show a concentration in the region downstream of the Sun due to gravitational focussing, there is a deficiency of particles in this spatial region in the intermediate size particles due to the filtering by the radiation pressure. The size of this avoidance region depends on β (and, hence, particle size and optical properties) and in three dimensions it has the approximate shape of a paraboloid. DDA can detect approximately 28 interstellar particles in this intermediate size range throughout quadrants III and IV in Fig. 1 during the entire mission. In quadrants I and II these particles are undetectable. A temporal variability is also evident in Fig. 17 with an increase in particle density at the boundary of the paraboloid between 2025 and 2029 due to the heliospheric filtering of the IMF which also affects the intermediate sized particles.

Finally, the spatial density of the smallest particles in our simulations having $r_d = 0.072\,\mu$m shows a strong temporal variation with an overall increase from 2025 to 2029. In this time interval the heliosphere gradually switches from its defocussing to its focussing configuration, leading to dust densities in the inner solar system increasing with time. Similar to the intermediate sized particles, these small particles are preferentially detectable in quadrants III and IV. The maximum focussing configuration is expected approximately in 2031, afterwards the IMF will become defocussing again (Strub et al., 2019). Hence, DDA measurements of such small interstellar particles should be concentrated towards the second half of the presently planned DESTINY$^+$ mission. The dust spatial density in the inner solar system still increases after the presently planned end of the mission (cf. Table 1).

4. Conclusions

We used two up-to-date computer models which are readily available to investigate the dynamics of interplanetary and interstellar dust particles in the inner heliosphere, namely IMEM developed by Dikarev et al. (2004, 2005a,c), and IMEX developed by Sterken et al. (2012, 2013) and Strub et al. (2019), which is based on the work of Landgraf (2000). We studied the detection conditions for such particles with a Dust Analyser (DDA) on board the DESTINY$^+$ mission to the active asteroid (3200) Phaethon. The mission is presently under development by the Japanese space agency JAXA/ISAS. The dust detection conditions during the Phaethon flyby were not the subject of this paper. Our results can be summarised as follows:

- The dust flux, average impact speed and impact direction of interplanetary and interstellar dust particles on to DDA are strongly variable in time. The modulation is largely due to the spacecraft motion around the Sun, but also due to size-dependent forces acting on the particles, leading to particle size-dependent variations in dust spatial density.
- A statistically significant number of interplanetary and interstellar dust particles can be detected and analysed in-situ with DDA during the interplanetary voyage of DESTINY$^+$ which is presently foreseen to last four years.
- During long mission periods the particle impact direction and speed can be used to discriminate between interstellar and interplanetary particles and likely also to distinguish between cometary and asteroidal particles.
- The average approach direction of small interstellar particles ($\lesssim 0.3\,\mu$m) is rather independent of particle size.
- Larger interstellar particles which are dominated by gravity can be preferentially detected in the focussing region downstream of the Sun.

Acknowledgements

HK gratefully acknowledges support from the Japan Society for the Promotion of Science (JSPS grant S16740) for a research visit at the Planetary Exploration Research Center at Chiba Institute of Technology during which a significant part of the work presented in this paper was performed. The IMEM and IMEX models were developed under ESA funding (contracts 21928/08/NL/AT and 4000106316/12/NL/AF - IMEX). Support by Deutsches Zentrum für Luft-und Raumfahrt (DLR, grant 50OO1801), by JAXA (grant UA18-DU2-03-U1000), and by MPS is also gratefully acknowledged. We thank Valery Dikarev, Alexey Mints and Rachel Soja for valuable discussions about the IMEM model. We are grateful to two anonymous referees whose comments substantially improved the presentation of our results.

Appendix 1

Figs. 11–15 show sky maps with fluxes and impact speeds for the asteroidal and cometary dust particles. To illustrate the variations during the DESTINY$^+$ mission we show sky maps for four different time intervals lasting 15 days each (Figs. 11–14), and for the total 1474 mission days (Fig. 15).

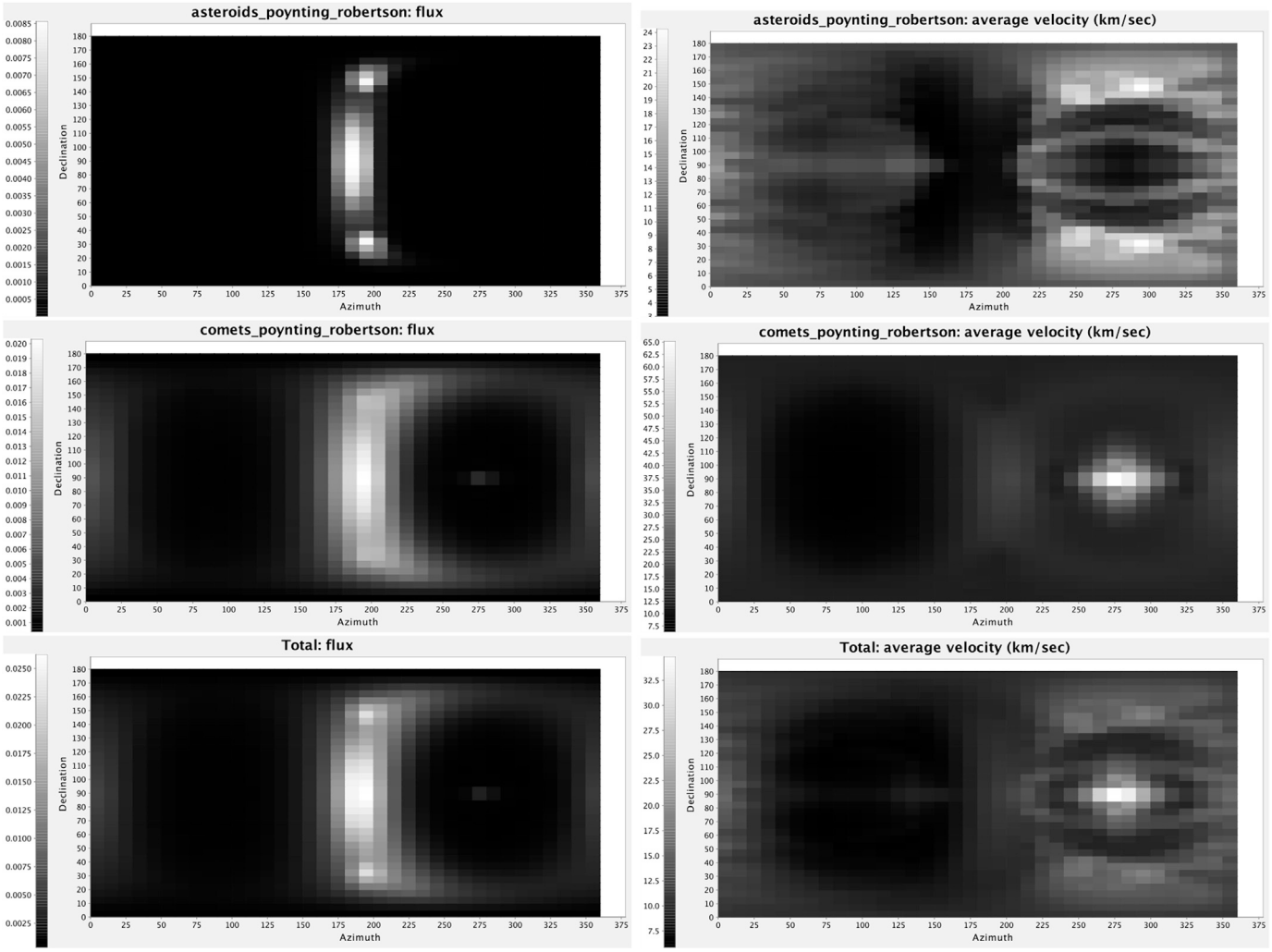

Fig. 11. Sky maps showing the distribution of dust fluxes (*left column*) and impact speeds (*right column*) for the time interval 01 to 15 December 2024. *Top row:* asteroidal particles (population 2), *Middle row*: cometary particles (population 4), *bottom row*: total fluxes (populations 2 and 4 together). The x axis shows the azimuth angle (ranging from 0 to 360°) and the y axis the declination (ranging from 0 to 180°). An azimuth angle 90° and declination 90° corresponds to the direction of vernal equinox. Due to the orientation of the DESTINY$^+$ trajectory, a declination of 90° is close to the ecliptic plane.

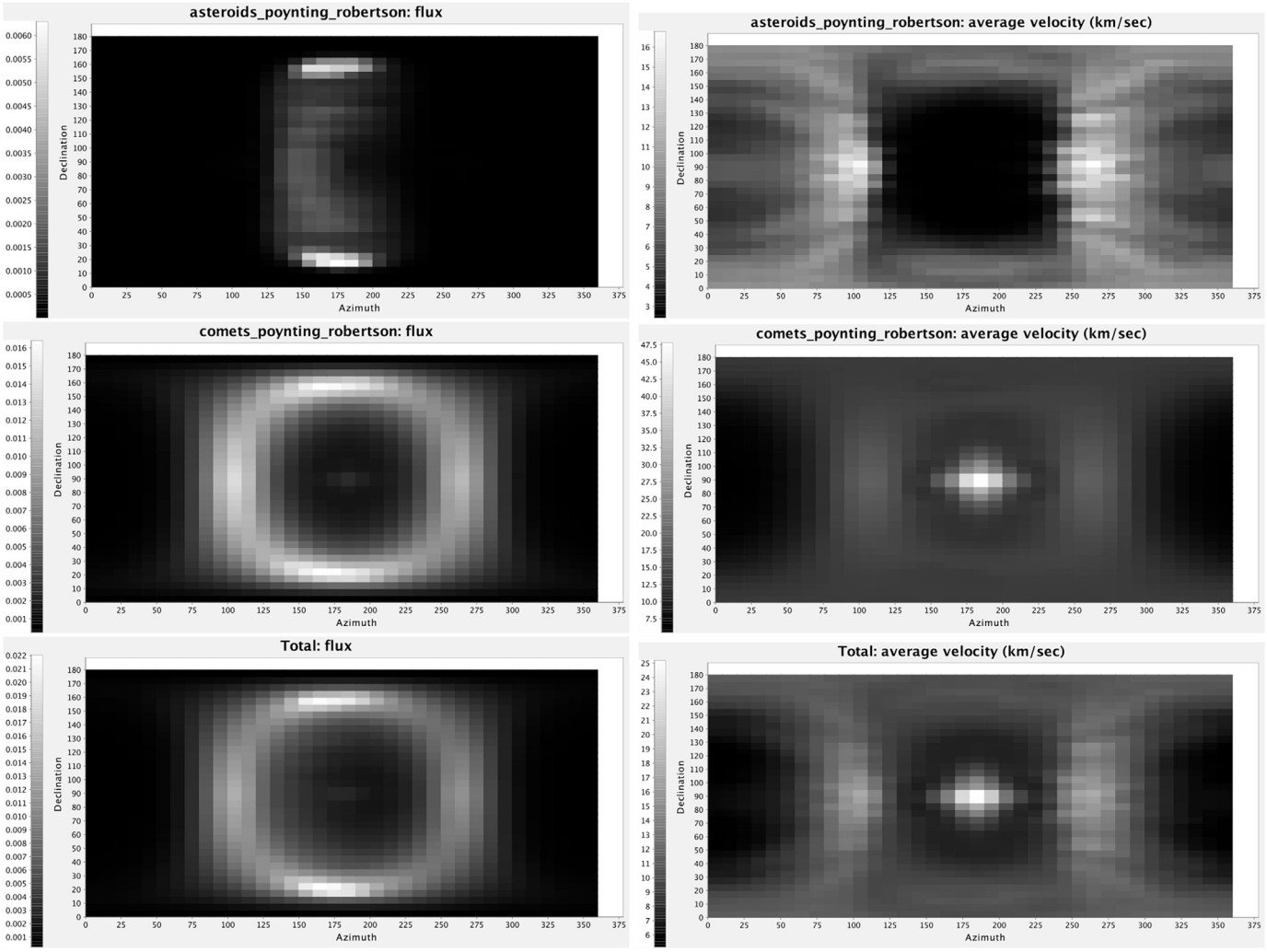

Fig. 12. Same as Fig. 11 but for the time interval 14 to 28 February 2025.

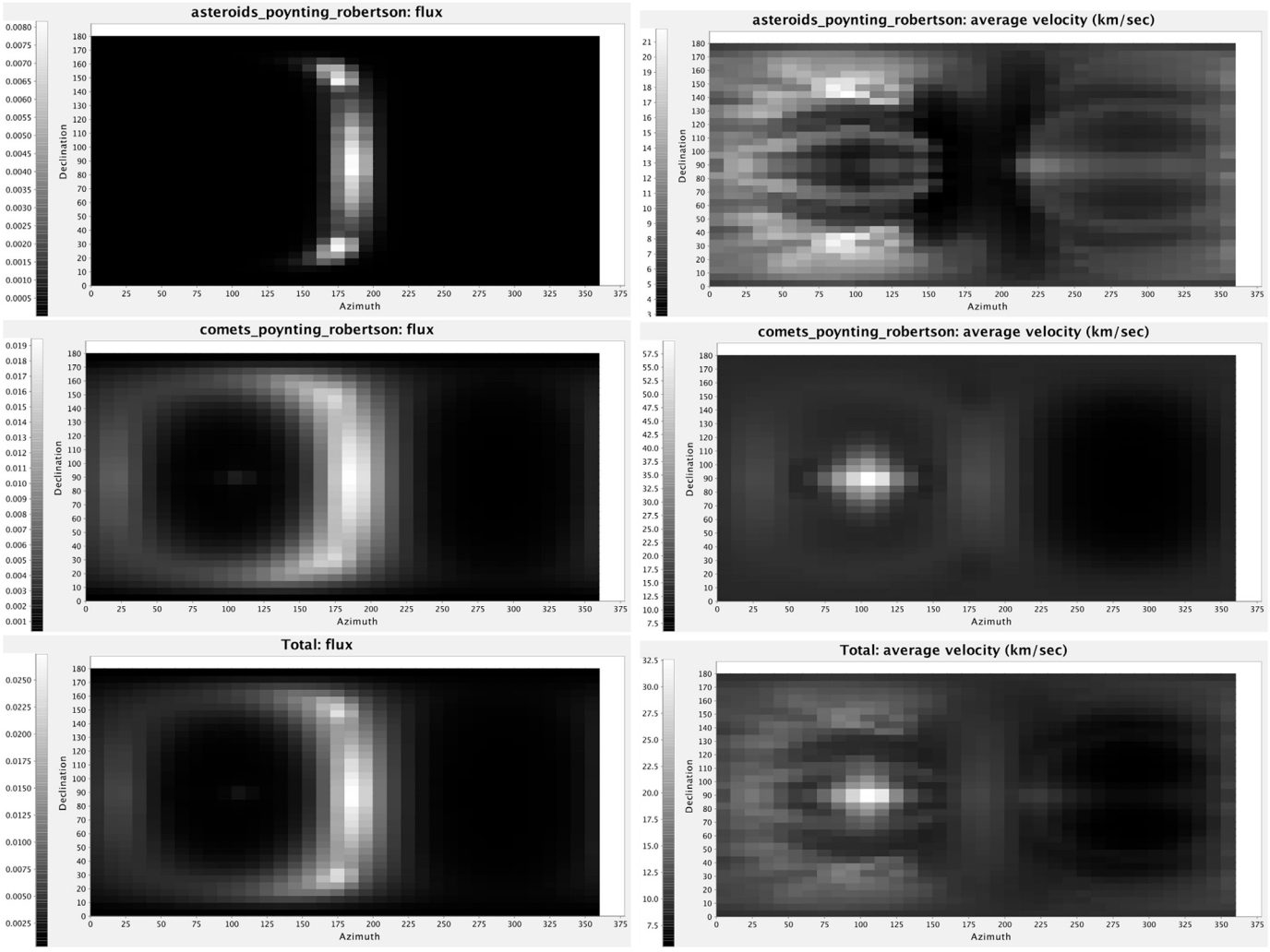

Fig. 13. Same as Fig. 11 but for the time interval 16 to 30 April 2025.

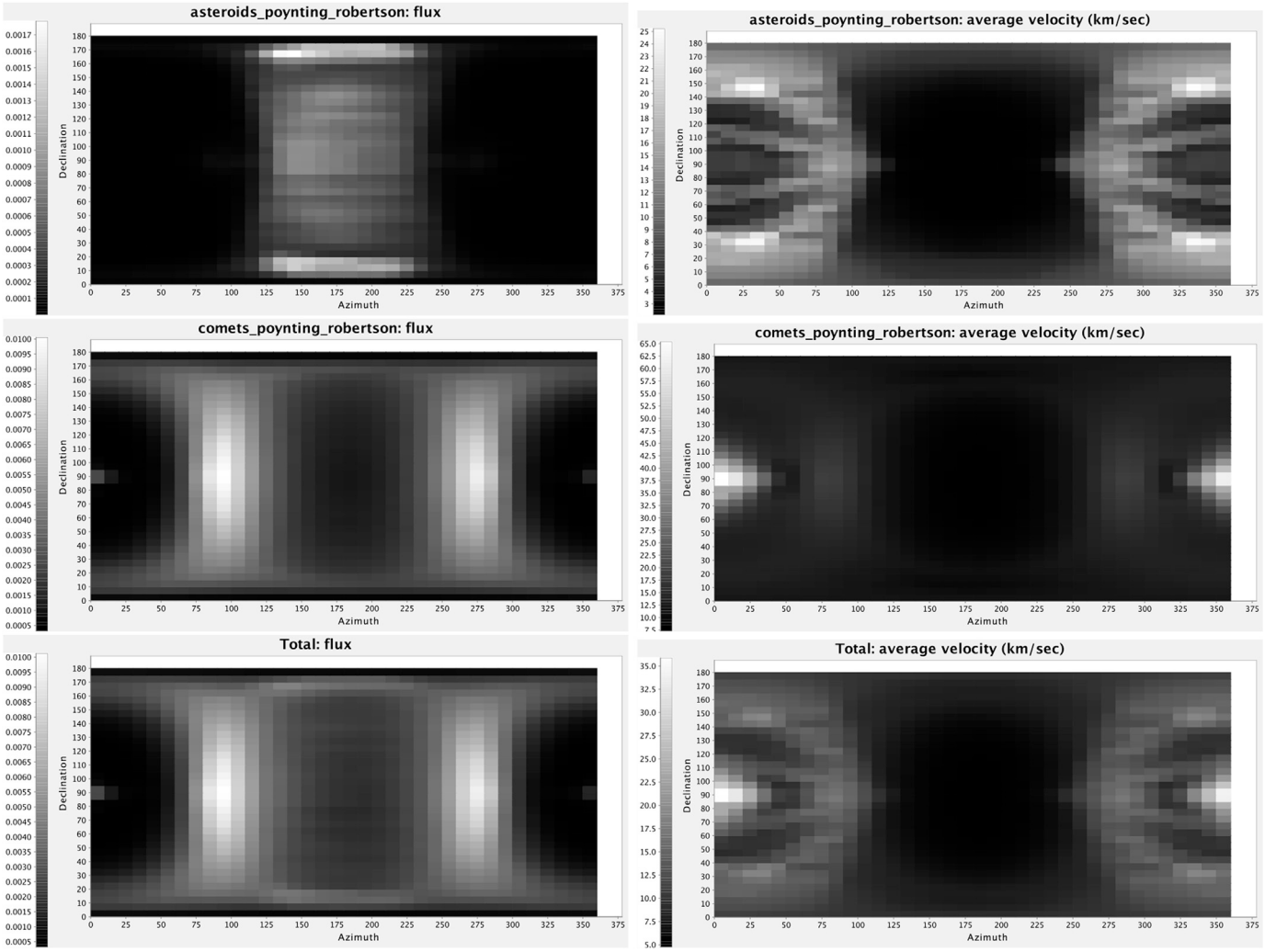

Fig. 14. Same as Fig. 11 but for the time interval 16 to 30 July 2025.

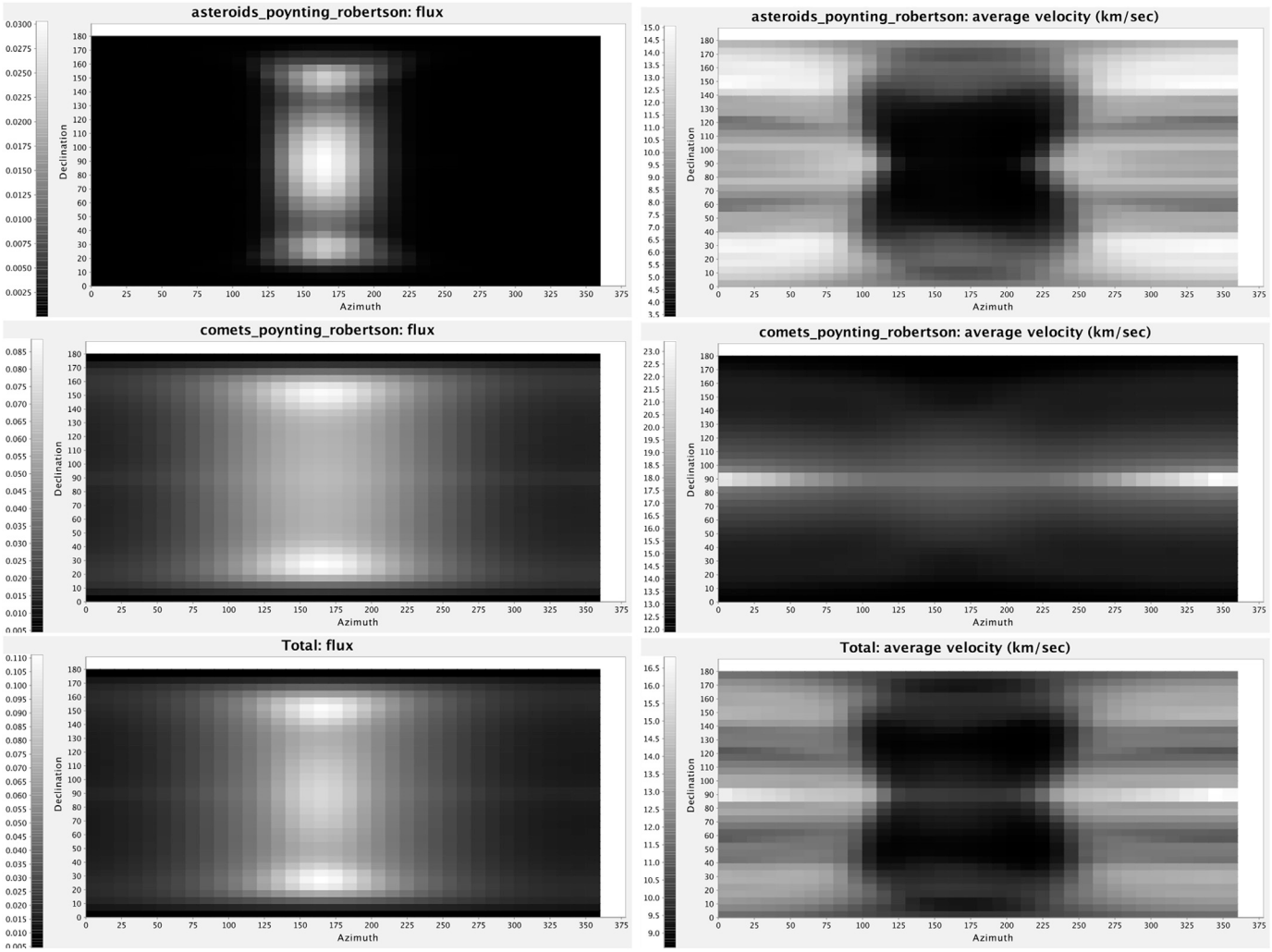

Fig. 15. Same as Fig. 11 but for the entire DESTINY^{+} mission.

Appendix 2

Figs. 16 to 18 show the spatial distribution of interstellar dust in the solar system from IMEX simulations for three particle sizes.

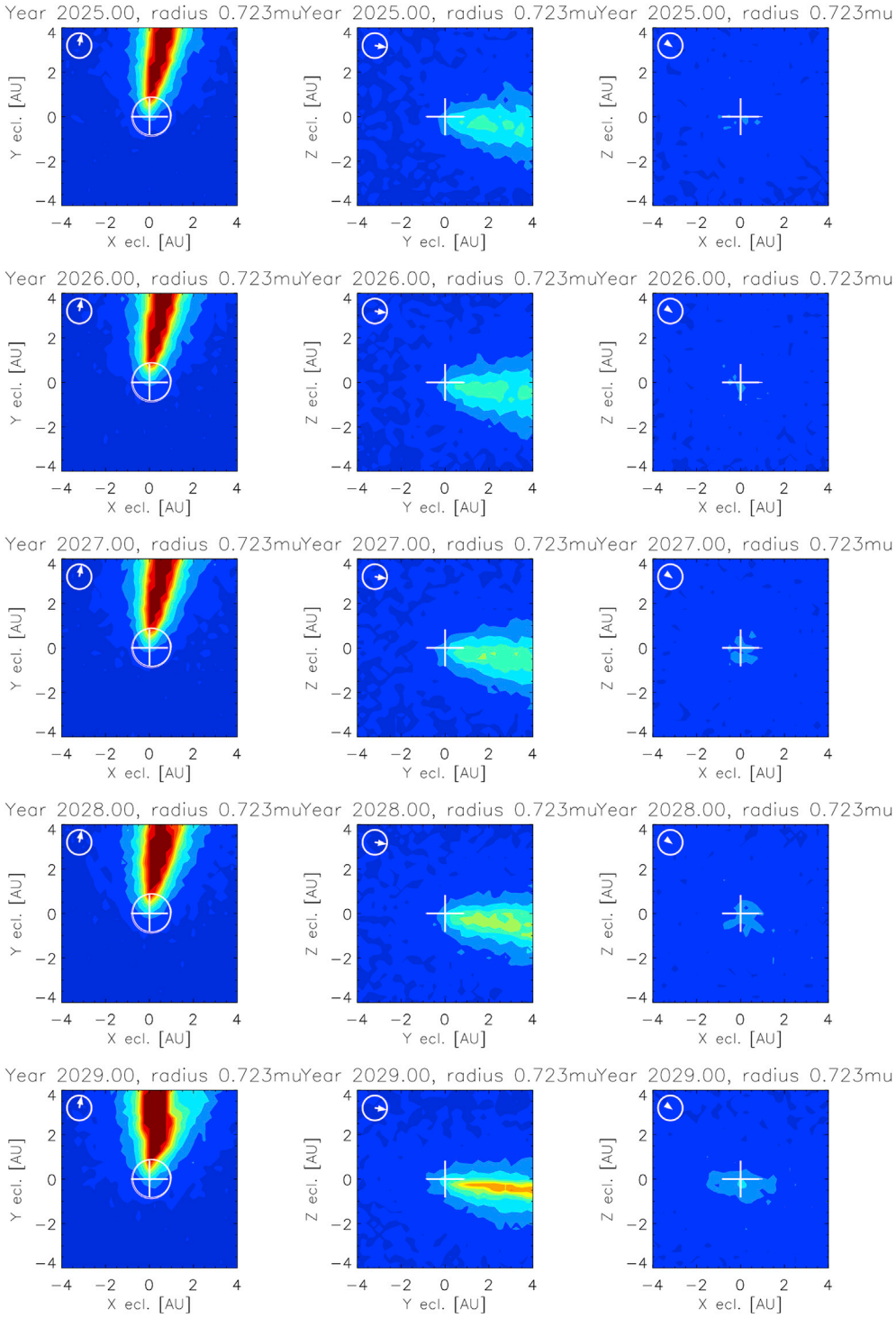

Fig. 16. Cross sections along the ecliptic coordinate planes through the simulated spatial density cubes for particles with radius $r_d = 0.723\,\mu$m during the DESTINY$^+$mission, at the beginning of each indicated year. The Sun is at the center, and the almost circular DESTINY$^+$trajectory is shown in white in the left column. The dust density is color coded: dark blue: low dust density; green, yellow, and red represent density enhancements with respect to the initial density at 50 AU. The projection of the original interstellar dust flow direction (at 50 AU) is shown as an arrow in the top left corner of each plot.

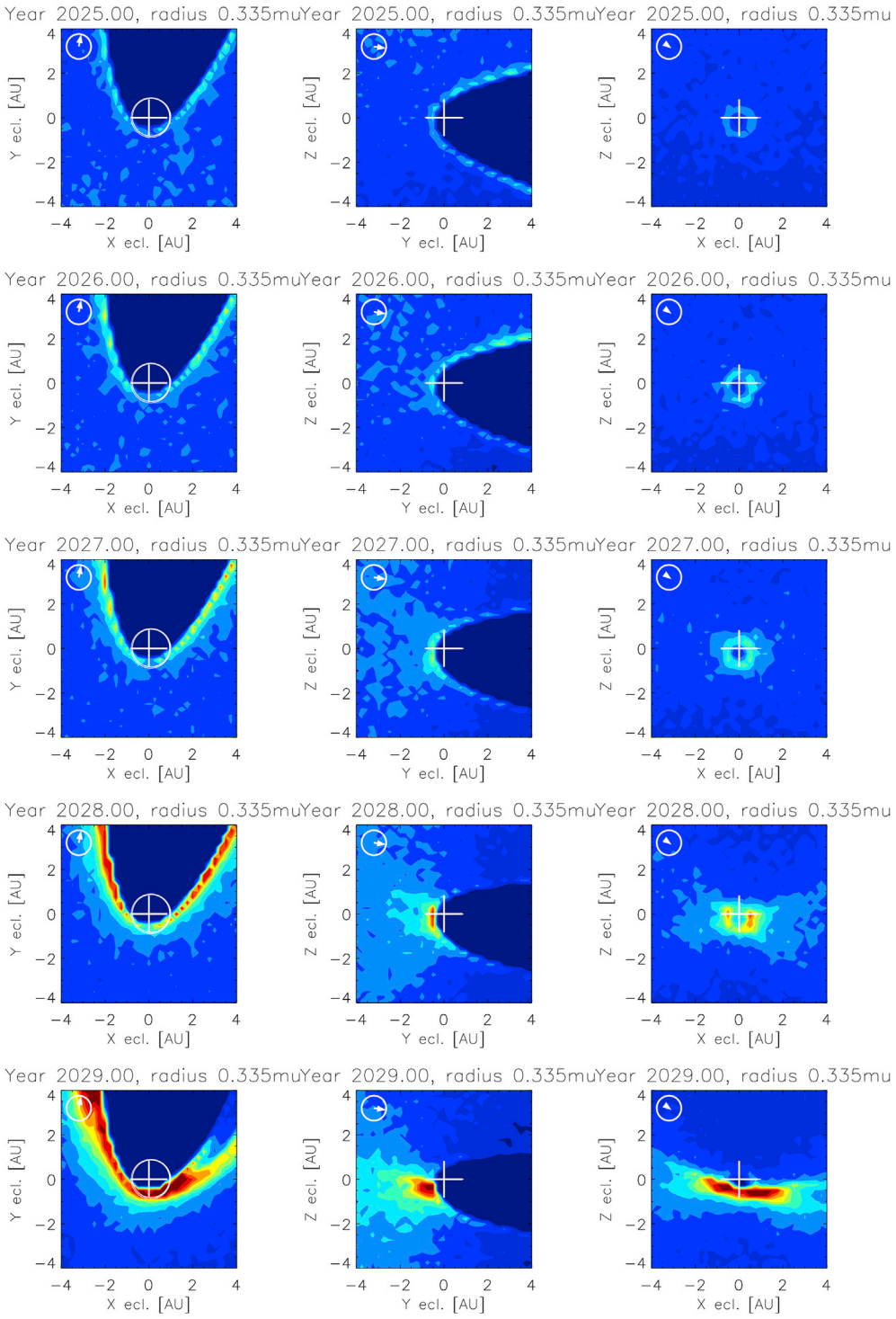

Fig. 17. Same as Fig. 18 but for particle radius $r_d = 0.335\ \mu$m.

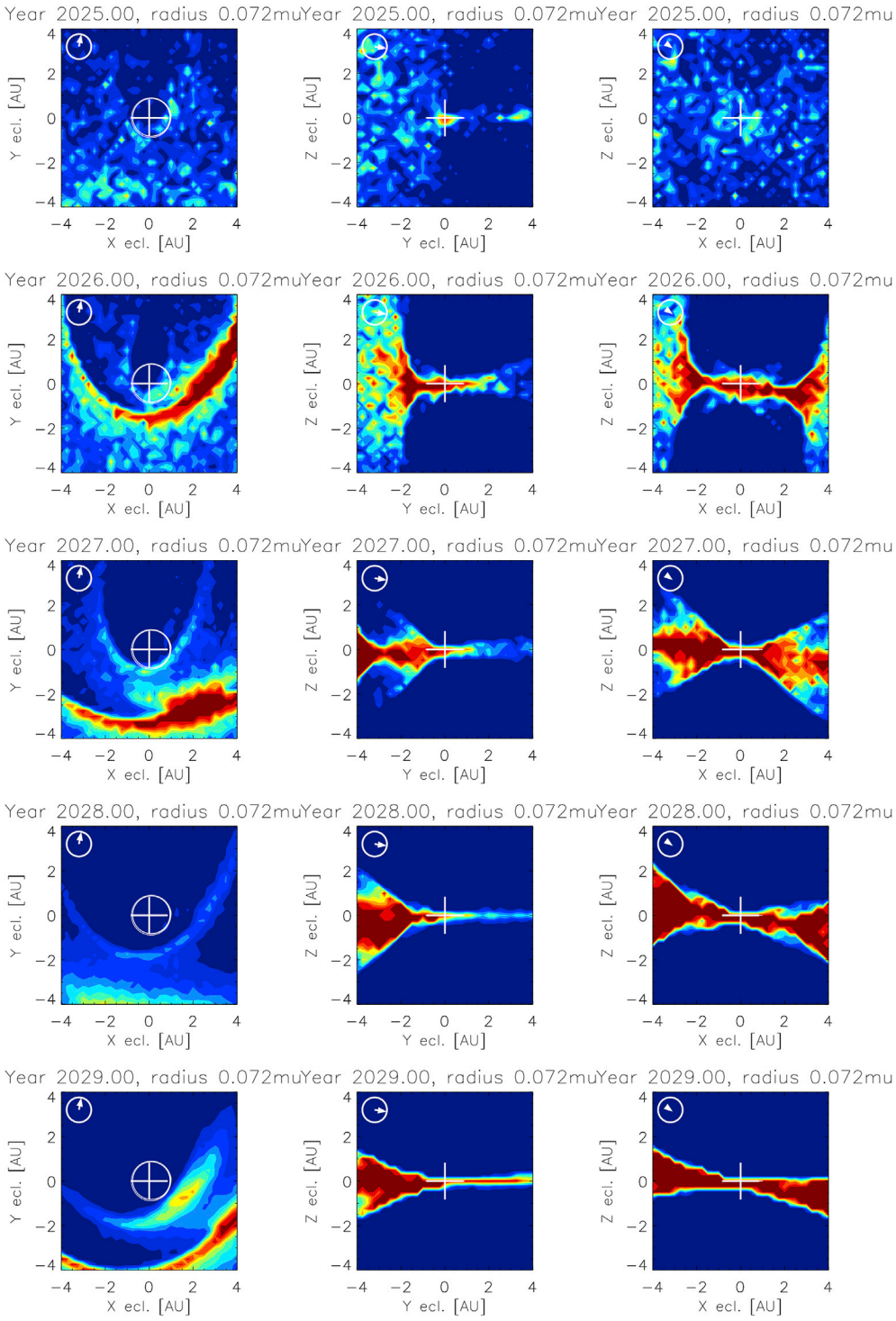

Fig. 18. Same as Fig. 18 but for particle radius $r_d = 0.072\,\mu$m.

References

Altobelli, N., Grün, E., Landgraf, M., 2006. A new look into the Helios dust experiment data: presence of interstellar dust inside the Earth's orbit. Astron. Astrophys. 448, 243–252.

Altobelli, N., Kempf, S., Krüger, H., Landgraf, M., Roy, M., Grün, E., 2005. Interstellar dust flux measurements by the Galileo dust instrument between Venus and Mars orbit. J. Geophys. Res. 110, 7102–7115.

Altobelli, N., Kempf, S., Landgraf, M., Srama, R., Dikarev, V., Krüger, H., Moragas-Klostermeyer, G., Grün, E., 2003. Cassini between venus and earth: detection of interstellar dust. J. Geophys. Res. 108 (A10), 7–1.

Altobelli, N., Postberg, F., Fiege, K., Trieloff, M., Kimura, H., Sterken, V.J., Hsu, H.-W., Hillier, J., Khawaja, N., Moragas-Klostermeyer, G., Blum, J., Burton, M., Srama, R., Kempf, S., Gruen, E., 2016. Flux and composition of interstellar dust at saturn from cassini's cosmic dust analyzer. Science 352, 312–318.

Arai, T., Kobayashi, M., Ishibashi, K., Yoshida, F., Kimura, H., Wada, K., Senshu, H., Yamada, M., Okudaira, O., Okamoto, T., Kameda, S., Srama, R., Krüger, H.,

Ishiguro, M., Yabuta, H., Nakamura, T., Watanabe, J., Ito, T., Ohtsuka, K., Tachibana, S., Mikouchi, T., Komatsu, M., Nakamura-Messenger, K., Sasaki, S., Hiroi, T., Abe, S., Urakawa, S., Hirata, N., Demura, H., Komatsu, G., Noguchi, T., Sekiguchi, T., Inamori, T., Yano, H., Yoshikawa, M., Ohtsubo, T., Okada, T., Iwata, T., Nishiyama, K., Toyota, H., Kawakatsu, Y., Takashima, T., 2018. Destiny$^+$ mission: flyby of geminids parent asteroid (3200) Phaethon and in-situ analyses of dust accreting on the earth. In: Lunar and Planetary Institute Science Conference Abstracts, Volume 49 of Lunar and Planetary Institute Science Conference Abstracts, p. 2570.

Bertaux, J.L., Blamont, J.F., 1976. Possible evidence for penetration of interstellar dust into the solar system. Nature 262, 263–266.

Dikarev, V., Grün, E., Baggaley, J., Galligan, D., Landgraf, M., Jehn, R., 2004. Modeling the sporadic meteoroid background cloud. Earth Moon Planets 95, 109–122.

Dikarev, V., Grün, E., Baggaley, J., Galligan, D., Landgraf, M., Jehn, R., 2005a. The new ESA meteoroid model. Adv. Space Res. 35, 1282–1289.

Dikarev, V., Grün, E., Baggaley, W.J., Galligan, D.P., Landgraf, M., Jehn, R., 2005b. A Single Physical Model for Diverse Meteoroid Data Sets. Technical Report. https://arxiv.org/abs/1902.02977.

Dikarev, V., Grün, E., Landgraf, M., Jehn, R., 2005c. Update of the ESA meteoroid model. In: Danesy, D. (Ed.), 4th European Conference on Space Debris, Volume 587 of ESA Special Publication, p. 271.

Koschny, D., Soja, R.H., Engrand, C., Flynn, G.J., Lasue, J., Levasseur-Regourd, A.-C., Malaspina, D., Nakamura, T., Poppe, A.-R., Sterken, V.J., Trigo-Rodríguez, J.M., 2019. Interplanetary dust, meteoroids, meteors and meteorites. Space Sci Rev. 215, 34. https://doi.org/10.1007/s11214-019-0597-7.

Frisch, P.C., Dorschner, J., Geiß, J., Greenberg, J.M., Grün, E., Landgraf, M., Hoppe, P., Jones, A.P., Krätschmer, W., Linde, T.J., Morfill, G.E., Reach, W.T., Slavin, J., Svestka, J., Witt, A., Zank, G.P., 1999. Dust in the local interstellar wind. Astrophys. J. 525, 492–516.

Frisch, P.C., Redfield, S., Slavin, J.D., 2011. The interstellar medium surrounding the sun. Annu. Rev. Astron. Astrophys. 49, 237–279.

Grün, E., Baguhl, M., Hamilton, D.P., Kissel, J., Linkert, D., Linkert, G., Riemann, R., 1995. Reduction of galileo and ulysses dust data. Planet. Space Sci. 43, 941–951.

Grün, E., Gustafson, B.E., Mann, I., Baguhl, M., Morfill, G.E., Staubach, P., Taylor, A., Zook, H.A., 1994. Interstellar dust in the heliosphere. Astron. Astrophys. 286, 915–924.

Grün, E., Srama, R., Krüger, H., Kempf, S., Dikarev, V., Helfert, S., Moragas-Klostermeyer, G., 2005. 2002 kuiper prize lecture: dust astronomy. Icarus 174, 1–14.

Grün, E., Zook, H.A., Baguhl, M., Balogh, A., Bame, S.J., Fechtig, H., Forsyth, R., Hanner, M.S., Horányi, M., Kissel, J., Lindblad, B.A., Linkert, D., Linkert, G., Mann, I., McDonnell, J.A.M., Morfill, G.E., Phillips, J.L., Polanskey, C., Schwehm, G.H., Siddique, N., Staubach, P., Svestka, J., Taylor, A., 1993. Discovery of Jovian dust streams and interstellar grains by the Ulysses spacecraft. Nature 362, 428–430.

Gustafson, B.A.S., 1994. Physics of zodiacal dust. Annu. Rev. Earth Planet Sci. 22, 553–595.

Hanuš, J., Delbo, M., Vokrouhlický, D., Pravec, P., Emery, J.P., Alí-Lagoa, V., Bolin, B., Devogèle, M., Dyvig, R., Galád, A., Jedicke, R., Kornoš, L., Kušnirák, P., Licandro, J., Reddy, V., Rivet, J.-P., Világi, J., Warner, B.D., 2016. Near-Earth asteroid (3200) Phaethon: characterization of its orbit, spin state, and thermophysical parameters. Astron. Astrophys. 592, A34.

Hillier, J.K., Green, S.F., McBride, N., Altobelli, N., Postberg, F., Kempf, S., Schwanethal, J., Srama, R., McDonnell, J.A.M., Grün, E., 2007. Interplanetary dust detected by the cassini CDA chemical analyser. Icarus 190, 643–654.

Hsieh, H.H., Jewitt, D., 2005. Search for activity in 3200 Phaethon. Astrophys. J. 624, 1093–1096.

Ishibashi, K., Kameda, S., Kagitani, M., Yamada, M., Okudaira, O., Okamoto, T., Arai, T., Yoshida, F., Ishimaru, T., Sato, S., Takashima, T., Iwata, T., Okada, T., Kimura, H., 2018. Telescopic camera for Phaethon (TCAP) and multiband camera for Phaethon (MCAP) to be installed on the Destiny+ spacecraft. In: Lunar and Planetary Institute Science Conference Abstracts, Volume 49 of Lunar and Planetary Institute Science Conference Abstracts, p. 2126.

Ito, T., Ishiguro, M., Arai, T., Imai, M., Sekiguchi, T., Bach, Y.P., Kwon, Y.G., Kobayashi, M., Ishimaru, R., Naito, H., Watanabe, M., Kuramoto, K., 2018. Extremely strong polarization of an active asteroid (3200) phaethon. Nat. Commun. 9, 2486.

Jewitt, D., Li, J., 2010. Activity in geminid parent (3200) Phaethon. Astron. J. 140, 1519–1527.

Jewitt, D., Li, J., Agarwal, J., 2013. The dust tail of asteroid (3200) Phaethon. Astrophys. J. Lett. 771, L36.

Kareta, T., Reddy, V., Hergenrother, C., Lauretta, D.S., Arai, T., Takir, D., Sanchez, J., Hanuš, J., 2018. Rotationally resolved spectroscopic characterization of near-earth object (3200) Phaethon. Astron. J. 156, 287.

Kawakatsu, Y., Itawa, T., 2013. Destiny mission overview: a small satellite mission for deep space exploration technology demonstration. Adv. Astronaut. Sci. 146, 12–585, 13.

Kempf, S., Srama, R., Altobelli, N., Auer, S., Tschernjawski, V., Bradley, J., Burton, M.E., Helfert, S., Johnson, T.V., Krüger, H., Moragas-Klostermeyer, G., Grün, E., 2004. Cassini between Earth and asteroid belt: first in-situ charge measurements of interplanetary grains. Icarus 171, 317–335.

Khawaja, N., 2016. Organic Compounds in Saturn's E-Ring and its Compositional Profile in the Vicinity of Rhea. PhD thesis. University of Heidelberg, Germany.

Kimura, H., 2015. Interstellar dust in the local cloud surrounding the sun. Mon. Not. R. Astron. Soc. 449, 2250–2258.

Kimura, H., 2017. High radiation pressure on interstellar dust computed by light-scattering simulation on fluffy agglomerates of magnesium-silicate grains with metallic-iron inclusions. Astrophys. J. Lett. 839, L23.

Kimura, H., Kobayashi, M., Wada, K., Arai, T., Ishiguro, M., Hanayama, H., Ishibashi, K., Hirai, T., Yoshida, F., Hong, P., 2019. On the detection of an ejecta dust cloud around asteroid (3200) Phaethon by the DESTINY$^+$ dust analyzer. I. Blackbody approximation. Planet. Space Sci. (submitted for publication.

Kimura, H., Mann, I., 1998. The electric charging of interstellar dust in the solar system and consequences for its dynamics. Astrophys. J. 499, 454–462.

Kimura, H., Mann, I., 1999. Radiation pressure on porous micrometeoroids. In: Baggaley, W.J., Porubcan, V. (Eds.), Meteroids 1998. Astronomical Institute of the Slovak Academy of Sciences, pp. 283–286.

Kimura, H., Mann, I., Jessberger, E.K., 2003a. Composition, structure, and size distribution of dust in the local interstellar cloud. Astrophys. J. 583, 314–321.

Kimura, H., Mann, I., Jessberger, E.K., 2003b. Elemental abundances and mass densities of dust and gas in the local interstellar cloud. Astrophys. J. 582, 846–858.

Kobayashi, M., Srama, R., Krüger, H., Arai, T., Kimura, H., 2018. Destiny$^+$ dust analyser. In: Lunar and Planetary Institute Science Conference Abstracts, Volume 49 of Lunar and Planetary Institute Science Conference Abstracts, 2050.

Krüger, H., Dikarev, V., Anweiler, B., Dermott, S.F., Graps, A.L., Grün, E., Gustafson, B.A., Hamilton, D.P., Hanner, M.M.S., Horányi, M., Kissel, J., Linkert, D., Linkert, G., Mann, I., McDonnell, J.A.M., Morfill, G.E., Polanskey, C., Schwehm, G.H., Srama, R., 2010. Three years of Ulysses dust data: 2005 to 2007. Planet. Space Sci. 58, 951–964.

Krüger, H., Landgraf, M., Altobelli, N., Grün, E., 2007. Interstellar dust in the solar system. Space Sci. Rev. 130, 401–408.

Krüger, H., Strub, P., Altobelli, N., Sterken, V., Srama, R., Grün, E., 2019. Interstellar dust in the solar system: Model versus in-situ spacecraft data. Astron. Astrophys. 626, A37 (2019). https://doi.org/10.1051/0004-6361/201834316.

Krüger, H., Strub, P., Sterken, V.J., Grün, E., 2015. Sixteen years of ulysses interstellar dust measurements in the solar system: I. mass distribution and gas-to-dust mass ratio. Astrophys. J. 812, 139.

Lallement, R., Bertaux, J.L., 2014. On the decades-long stability of the interstellar wind through the solar system. Astron. Astrophys. 565, A41.

Landgraf, M., 1998. Modellierung der Dynamik und Interpretation der In-situ-Messung interstellaren Staubs in der lokalen Umgebung des Sonnensystems. PhD thesis. Ruprecht-Karls-Universität Heidelberg.

Landgraf, M., 2000. Modelling the motion and distribution of interstellar dust inside the heliosphere. J. Geophys. Res. 105 (A5:10), 303–10316.

Landgraf, M., Augustsson, K., Grün, E., Gustafson, B.A.S., 1999. Deflection of the local interstellar dust flow by solar radiation pressure. Science 322, 286:2,319–2.

Landgraf, M., Baggeley, W.J., Grün, E., Krüger, H., Linkert, G., 2000. Aspects of the mass distribution of interstellar dust grains in the solar system from in situ measurements. J. Geophys. Res. 105, 343–10352. A5:10.

Landgraf, M., Krüger, H., Altobelli, N., Grün, E., 2003. Penetration of the Heliosphere by the interstellar dust stream during solar maximum. J. Geophys. Res. 108, 5–1.

Landgraf, M., Liou, J., Zook, H., Gruen, E., 2002. Origins of solar system dust beyond Jupiter. Astron. J. 123, 2857–2861.

Li, J., Jewitt, D., 2013. Recurrent perihelion activity in (3200) Phaethon. Astron. J. 145, 154.

Licandro, J., Campins, H., Mothé-Diniz, T., Pinilla-Alonso, N., de León, J., 2007. The nature of comet-asteroid transition object (3200) Phaethon. Astron. Astrophys. 461, 751–757.

Linde, T.J., Gombosi, T.I., 2000. Interstellar dust filtration at the heliospheric interface. J. Geophys. Res. 105, 10411–10418.

Ma, Q., Matthews, L.S., Land, V., Hyde, T.W., 2013. Charging of aggregate grains in astrophysical environments. Astrophys. J. 763, 77.

Mann, I., 2010. Interstellar dust in the solar system. Annu. Rev. Astron. Astrophys. 48, 173–203.

McComas, D.J., Bzowski, M., Fuselier, S.A., Frisch, P.C., Galli, A., Izmodenov, V.V., Katushkina, O.A., Kubiak, M.A., Lee, M.A., Leonard, T.W., Möbius, E., Park, J., Schwadron, N.A., Sokol, J.M., Swaczyna, P., Wood, B.E., Wurz, P., 2015. Local interstellar medium: six years of direct sampling by ibex. Astrophysical Journal, Supplement 220, 22.

Mukai, T., 1981. On the charge distribution of interplanetary grains. Astron. Astrophys. 99, 1–6.

Nesvorný, D., Jenniskens, P., Levison, H.F., Bottke, W.F., Vokrouhlický, D., Gounelle, M., 2010. Cometary origin of the zodiacal cloud and carbonaceous micrometeorites. Implications for hot debris disks. Astrophys. J. 713, 816–836.

Pokorný, P., Vokrouhlický, D., Nesvorný, D., Campbell-Brown, M., Brown, P., 2014. Dynamical model for the toroidal sporadic meteors. Astrophys. J. 789, 25.

Sarli, B.V., Horikawa, M., Yam, C.H., Kawakatsu, Y., Yamamoto, T., 2018. Destiny$^+$ trajectory design to (3200) Phaethon. J. Astronaut. Sci. 65, 82–110.

Sarli, B.V., Yam, C.H., Horikawa, M., Kawakatsu, Y., 2016. Low-thrust trajectory design for the DESTINY mission to (3200) Phaethon. In: 26th AAS/AIAA Space Flight Mechanics Meeting, Napa, CA, USA, AAS:16–387.

Slavin, J.D., Frisch, P.C., 2008. The boundary conditions of the heliosphere: photoionization models constrained by interstellar and in situ data. Astron. Astrophys. 491, 53–68.

Slavin, J.D., Frisch, P.C., Müller, H.-R., Heerikhuisen, J., Pogorelov, N.V., Reach, W.T., Zank, G., 2012. Trajectories and distribution of interstellar dust grains in the heliosphere. Astrophys. J. 760, 46.

Srama, R., 2009. Cassini-Huygens and beyond - Tools for Dust Astronomy. Habilitation Thesis, Universität Stuttgart.

Srama, R., Ahrens, T.J., Altobelli, N., Auer, S., Bradley, J.G., Burton, M., Dikarev, V.V., Economou, T., Fechtig, H., Görlich, M., Grande, M., Graps, A.L., Grün, E., Havnes, O., Helfert, S., Horányi, M., Igenbergs, E., Jeßberger, E.K., Johnson, T.V., Kempf, S., Krivov, A.V., Krüger, H., Moragas-Klostermeyer, G., Lamy, P., Landgraf, M., Linkert, D., Linkert, G., Lura, F., Mocker-Ahlreep, A., McDonnell, J.A.M., Möhlmann, D., Morfill, G.E., Müller, M., Roy, M., Schäfer, G., Schlotzhauer, G.H.,

Schwehm, G.H., Spahn, F., Stübig, M., Svestka, J., Tschernjawski, V., Tuzzolino, A.J., Wäsch, R., Zook, H.A., 2004. The cassini cosmic dust analyzer. Space Sci. Rev. 114, 465–518.

Srama, R., Kempf, S., Moragas-Klostermeyer, G., Altobelli, N., Auer, S., Beckmann, U., Bugiel, S., Burton, M., Economou, T., Fechtig, H., Fiege, K., Green, S.F., Grande, M., Havnes, O., Hillier, J.K., Helfert, S., Horanyi, M., Hsu, S., Igenbergs, E., Jessberger, E.K., Johnson, T.V., Khalisi, E., Krüger, H., Matt, G., Mocker, A., Lamy, P., Linkert, G., Lura, F., Möhlmann, D., Morfill, G., Otto, K., Postberg, F., Roy, M., Schmidt, J., Schwehm, G.H., Spahn, F., Sterken, V., Svestka, J., Tschernjawski, V., Grün, E., Röser, H.-P., 2011. The cosmic dust analyser onboard CASSINI: ten years of discoveries. CEAS Space Journal 2, 3–16.

Sterken, V.J., Altobelli, N., Kempf, S., Krüger, H., Srama, R., Strub, P., Grün, E., 2013. The filtering of interstellar dust in the solar system. Astron. Astrophys. 552, A130.

Sterken, V.J., Altobelli, N., Kempf, S., Schwehm, G., Srama, R., Grün, E., 2012. The flow of interstellar dust into the solar system. Astron. Astrophys. 538, A102.

Sterken, V.J., Strub, P., Krüger, H., von Steiger, R., Frisch, P., 2015. Sixteen years of ulysses interstellar dust measurements in the solar system: III. Simulations and data unveil new insights into local interstellar dust. Astrophys. J. 812, 141.

Sterken, V.J., Westphal, A.J., Altobelli, N., Grün, E., Hillier, J.K., Postberg, F., Srama, R., Allen, C., Anderson, D., Ansari, A., Bajt, S., Bastien, R.S., Bassim, N., Bechtel, H.A., Borg, J., Brenker, F.E., Bridges, J., Brownlee, D.E., Burchell, M., Burghammer, M., Butterworth, A.L., Changela, H., Cloetens, P., Davis, A.M., Doll, R., Floss, C., Flynn, G., Frank, D., Gainsforth, Z., Heck, P.R., Hoppe, P., Hudson, B., Huth, J., Hvide, B., Kearsley, A., King, A.J., Lai, B., Leitner, J., Lemelle, L., Leroux, H., Leonard, A., Lettieri, R., Marchant, W., Nittler, L.R., Ogliore, R., Ong, W.J., Price, M.C., Sandford, S.A., Tresseras, J.-A.S., Schmitz, S., Schoonjans, T., Silversmit, G., Simionovici, A., Solé, V.A., Stephan, T., Stodolna, J., Stroud, R.M., Sutton, S., Trieloff, M., Tsou, P., Tsuchiyama, A., Tyliszczak, T., Vekemans, B., Vincze, L., von Korff, J., Wordsworth, N., Zevin, D., Zolensky, M.E., 2014. Stardust Interstellar Preliminary Examination X: impact speeds and directions of interstellar grains on the Stardust dust collector. Meteorit. Planet. Sci. 49, 1680–1697.

Sterken, V.J., Westphal, A.J., N, A., D, M., P, F., 2019. Interstellar dust in the solar system. Space Sci. Rev. (in press).

Strub, P., Krüger, H., Sterken, V.J., 2015. Sixteen years of Ulysses interstellar dust measurements in the Solar System: II. Fluctuations in the dust flow from the data. Astrophys. J. 812, 140.

Strub, P., Sterken, V.J., Soja, R., Krüger, H., Grün, Srama, R., 2019. Heliospheric modulation of the interstellar dust flow on to Earth. Astron. Astrophys. 621, A54.

Swaczyna, P., Bzowski, M., Kubiak, M.A., Sokół, J.M., Fuselier, S.A., Galli, A., Heirtzler, D., Kucharek, H., McComas, D.J., Möbius, E., Schwadron, N.A., Wurz, P., 2018. Interstellar neutral helium in the heliosphere from IBEX observations. V. Observations in IBEX-lo ESA steps 1, 2, and 3. Astrophys. J. 854, 119.

Szalay, J.-R., Pokorny, P., Horányi, M., Janches, D., Sarantos, M., Srama, R., 2019. Impact ejecta environment of an eccentric asteroid: 3200 Phaethon. Planet. Space Sci. 165, 194–204.

Takir, D., Reddy, V., Hanus, J., Arai, T., Lauretta, D.S., Kareta, T., Howell, E.S., Emery, J.P., McGraw, L.E., 2018. Spectroscopy of asteroid (3200) Phaethon: implications for B-asteroids. In: Lunar and Planetary Science Conference, Volume 49 of Lunar and Planetary Science Conference, p. 2624.

Taylor, P.A., Marshall, S.E., Venditti, F., Virkki, A.K., Benner, L.A.M., Brozovic, M., Naidu, S.P., Howell, E.S., Kareta, T.R., Reddy, V., Takir, D., Rivkin, A.S., Zambrano-Marin, L.F., Bhiravarasu, S.S., Rivera-Valentin, E.G., Aponte-Hernandez, B., Rodriguez Sanchez-Vahamonde, C., Nolan, M.C., Giorgini, J.D., Vervack, R.J., Fernandez, Y.R., Crowell, J.L., Lauretta, D.S., Arai, T., 2018. Radar and infrared observations of near-earth asteroid 3200 Phaethon. In: Lunar and Planetary Science Conference, Volume 49 of Lunar and Planetary Science Conference, p. 2509.

Tielens, A.G.G.M., 2005. The Physics and Chemistry of the Interstellar Medium. Cambridge University Press, Cambridge, UK, ISBN 0521826349.

Westphal, A.J., Stroud, R.M., Bechtel, H.A., Brenker, F.E., Butterworth, A.L., Flynn, G.J., Frank, D.R., Gainsforth, Z., Hillier, J.K., Postberg, F., Simionovici, A.S., Sterken, V.J., Nittler, L.R., Allen, C., Anderson, D., Ansari, A., Bajt, S., Bastien, R.K., Bassim, N., Bridges, J., Brownlee, D.E., Burchell, M., Burghammer, M., Changela, H., Cloetens, P., Davis, A.M., Doll, R., Floss, C., Grün, E., Heck, P.R., Hoppe, P., Hudson, B., Huth, J., Kearsley, A., King, A.J., Lai, B., Leitner, J., Lemelle, L., Leonard, A., Leroux, H., Lettieri, R., Marchant, W., Ogliore, R., Ong, W.J., Price, M.C., Sandford, S.A., Sans Tresseras, J.A., Schmitz, S., Schoonjans, T., Schreiber, K., Silversmit, G., Solé, V.A., Srama, R., Stadermann, F.J., Stephan, T., Stodolna, J., Sutton, S., Trieloff, M., Tsou, P., Tyliszczak, T., Vekemans, B., Vincze, L., Von Korff, J., Wordsworth, N., Zevin, D., Zolensky, M.E., 30714 Stardust@home dusters, 2014. Evidence for interstellar origin of seven dust particles collected by the Stardust spacecraft. Science 345, 786–791.

Witte, M., Banaszkiewicz, H., Rosenbauer, H., 1996. Recent results on the parameters of interstellar helium from the Ulysses/GAS experiment. Space Sci. Rev. 78 (1/2), 289–296.

Witte, M., Banaszkiewicz, M., Rosenbauer, H., McMullin, D., 2004. Kinetic parameters of interstellar neutral helium: updated results from the Ulysses/GAS instrument. Adv. Space Res. 34, 61–65.

Wood, B.E., Müller, H.-R., Witte, M., 2015. Revisiting ulysses observations of interstellar helium. Astrophys. J. 801, 62+.

Ye, Q., Wiegert, P.A., Hui, M.-T., 2018. In search of recent disruption of (3200) Phaethon: model implication and hubble space telescope search. Astrophys. J. Lett. 864, L9.